HAL
open science

Surface displacements on faults triggered by slow magma transfers between dyke injections in the 2005–2010 rifting episode at Dabbahu–Manda–Hararo rift (Afar, Ethiopia)

S. Dumont, A. Socquet, R. Grandin, Cécile Doubre, Y. Klinger

To cite this version:

S. Dumont, A. Socquet, R. Grandin, Cécile Doubre, Y. Klinger. Surface displacements on faults triggered by slow magma transfers between dyke injections in the 2005–2010 rifting episode at Dabbahu–Manda–Hararo rift (Afar, Ethiopia). Geophysical Journal International, 2016, 204 (1), pp.399-417. 10.1093/gji/ggv449 . hal-01862661

HAL Id: hal-01862661

https://hal.science/hal-01862661v1

Submitted on 27 Aug 2018

HAL is a multi-disciplinary open access archive for the deposit and dissemination of scientific research documents, whether they are published or not. The documents may come from teaching and research institutions in France or abroad, or from public or private research centers.

L'archive ouverte pluridisciplinaire **HAL**, est destinée au dépôt et à la diffusion de documents scientifiques de niveau recherche, publiés ou non, émanant des établissements d'enseignement et de recherche français ou étrangers, des laboratoires publics ou privés.

Geophysical Journal International

Geophys. J. Int. (2016) **204,** 399–417
GJI Geodynamics and tectonics

doi: 10.1093/gji/ggv449

Surface displacements on faults triggered by slow magma transfers between dyke injections in the 2005–2010 rifting episode at Dabbahu–Manda–Hararo rift (Afar, Ethiopia)

S. Dumont,[1,2] A. Socquet,[3] R. Grandin,[2] C. Doubre[4] and Y. Klinger[2]

[1]*Nordic Volcanological Center, Institute of Earth Sciences, University of Iceland, IS-*101 *Reykjavík, Iceland. E-mail: sd@hi.is*
[2]*Institut de Physique du Globe de Paris, Paris Sorbonne Cité, Univ. Diderot, UMR*7154*—CNRS, Tectonique et Mécanique de la Lithosphère,* 1 *rue Jussieu, F-*75005 *Paris, France*
[3]*Université Grenoble Alpes, ISTerre, CNRS, F-*38041 *Grenoble, France*
[4]*IPGS, Université de Strasbourg/EOST, CNRS* 5 *rue Descartes, F-*67084 *Strasbourg Cedex, France*

Accepted 2015 October 14. Received 2015 October 13; in original form 2014 November 30

SUMMARY

The rifting episode that occurred in Dabbahu–Manda–Hararo (Ethiopia) between 2005 and 2010 during which 14 dyke intrusions were emitted, was a unique opportunity to study interactions between tectonic deformation and magmatic processes. While magmatism has been shown to control primarily the spatial and temporal distribution of dyke intrusions during this accretion sequence, the role of faults in accommodating plate spreading in rift segments is poorly understood. During interdyking periods, transient ground deformation due to magma movement is generally observed. Investigating such a small-scale deformation and in particular the movement along faults during these periods will help understanding the factors that trigger fault movement in magmatic rifts. We analyse fault activity during three interdyking periods: 2006 December–June (d0–d1), 2007 January–July (d5–d6) and 2009 November–January (d10–d11). The time–space evolution of surface displacements along ∼700 faults is derived from pairs of ascending and descending SAR interferograms. Surface slip distributions are then compared with codyking ground deformation fields. The results show that faults are mainly activated above the areas affected by magma emplacement during interdyking periods. A detailed analysis of brittle deformation during the six months following the 2005 September intrusion shows asymmetric deformation on the rift shoulders, with significant opening on faults located to the west of the dyke. We explain this feature by the activation of westward dipping pre-existing faults, with block rotations in between. In addition, we observe that the strip encompassing the activated faults narrows by 30 per cent from co- to interdyking period. This suggests that magma keeps migrating to shallower depths after the dyke intrusion. During a rifting episode, activation of faults in a pre-existing fracture network therefore seems to be mainly controlled by deep magma processes.

Key words: Transient deformation; Radar interferometry; Creep and deformation; Continental margins: divergent; Dynamics and mechanics of faulting; Magma chamber processes.

1 INTRODUCTION

Stress accumulated along divergent boundaries particularly at oceanic spreading centres is mainly released during rifting episodes (Björnsson & Saemundsson 1977; Björnsson 1985; Blackman *et al.* 2000; Dziak *et al.* 2004; Buck *et al.* 2006; Hamling *et al.* 2009, 2010; Grandin *et al.* 2010b). When magma is available, dyke intrusions appear more efficient than faulting at releasing stress and balancing the deficit of opening (Björnsson & Saemundsson 1977; Björnsson 1985; Buck 2006). As suggested by the south–north evolution of the along-axis segmentation of the East African Rift, that is from the continental domain to the most evolved rift segments in Afar, magma processes with dyke intrusions also characterize late phases of the continental rifting (Hayward & Ebinger 1996). In this region, although dyke intrusions may release 80 per cent of the accumulated stresses, the current surface topography is mainly dominated by normal faulting (Manighetti *et al.* 1998; Ebinger & Casey 2001). Furthermore, most dykes which do not reach the surface are associated with movement on normal faults, as observed during the previous rifting episodes both in Iceland and in Afar with vertical displacements ranging from 0.8 m to 5 m for the largest intrusions (Björnsson & Saemundsson 1977;

© The Authors 2015. Published by Oxford University Press on behalf of The Royal Astronomical Society.

Downloaded from http://gji.oxfordjournals.org/ by guest on November 26, 2015

Le Dain *et al.* 1979; Ruegg *et al.* 1979; Yirgu *et al.* 2006; Rowland *et al.* 2007).

The shape of the current topography in Afar results from a complex competition between a persistent faulting activity and intermittent effusions of lava (De Chabalier & Avouac 1994; Manighetti *et al.* 2001; Lahitte *et al.* 2003a). As a consequence, it is difficult to decipher the respective role of faulting versus magmatism, especially as faulting is itself largely controlled by magmatism. So far, studies that have investigated the relationship between magmatic intrusions and fault growth in a rift (Mastin & Pollard 1988; Rubin 1992; Gudmundsson 2003; Lahitte *et al.* 2003b; Gudmundsson & Loetveit 2005; Singh *et al.* 2006; Valentine & Krogh 2006; Calais *et al.* 2008; Biggs *et al.* 2009; Baer & Hamiel 2010; Magee *et al.* 2013; Medynski *et al.* 2013), have focused on dyke injection mechanisms during discrete intrusion events (Björnsson & Saemundsson 1977; Einarsson & Brandsdottir 1980; Björnsson *et al.* 1979; Björnsson 1985; Abdallah *et al.* 1979; Ruegg *et al.* 1979; Lépine *et al.* 1980; Tarantola *et al.* 1979, 1980; Tryggvason 1984; Einarsson 1991; Buck *et al.* 2006; Wright *et al.* 2006; Yirgu *et al.* 2006; Ayele *et al.* 2007; Barisin *et al.* 2009; Grandin *et al.* 2009, 2010b, 2011; Hamling *et al.* 2009, 2010; Keir *et al.* 2009; Nooner *et al.* 2009; Belachew *et al.* 2011, 2013). The Dabbahu–Manda–Hararo (DMH) rifting episode was monitored using an unprecedented amount of Envisat SAR images allowing numerous studies on the intrusive sequence and the induced stress changes (Ayele *et al.* 2007; Grandin *et al.* 2009, 2010a, 2010b; Hamling *et al.* 2009, 2010) but also on the post-rifting deformation and the related processes of deformation, such as viscoelastic relaxation (Cattin *et al.* 2005; Nooner *et al.* 2009; Grandin *et al.* 2010a; Hamling *et al.* 2014; Pagli *et al.* 2014). This data set represents an excellent opportunity to monitor the displacements across and along the faults in details throughout a major magmatic episode. It therefore provides an approach complementary to previous studies and also crucial insights into the magmato-tectonic interactions occurring along an opening segment.

Using the interferometric synthetic aperture radar (InSAR) method, the aim of this paper is to study faulting and its interaction with crustal magma processes during a rifting episode. We investigate three interdyking periods spanning between two and six months after the 2005 September, 2007 January and 2008 October intrusions (Fig. 1c). Each of these interdyking periods is imaged by several ascending and descending interferograms, allowing us to derive the space and time evolution of fault displacements and to compare it with transient deformation related to magma transfers. Finally, we investigate further the magmato-tectonic interactions due to the 2005 September intrusion.

2 TECTONIC SETTING

The DMH rift is located in the Afar depression where three divergent plate boundaries meet: the Red Sea ridge (RSR), the Gulf of Aden ridge and the East African Rift Systems (EARS; Fig. 1a). For the last ~3 Myr, faulting and volcanism have taken place along ~60 km-long and ~20 km-wide aligned volcano-tectonic rift segments. Their size and morphology are similar to those of the second-order segmentation of the oceanic slow-spreading ridges (Hayward & Ebinger 1996; Manighetti *et al.* 1998), while the continental breakup has not yet been established (Makris & Ginzburg 1987; Tiberi *et al.* 2005; Hammond *et al.* 2011).

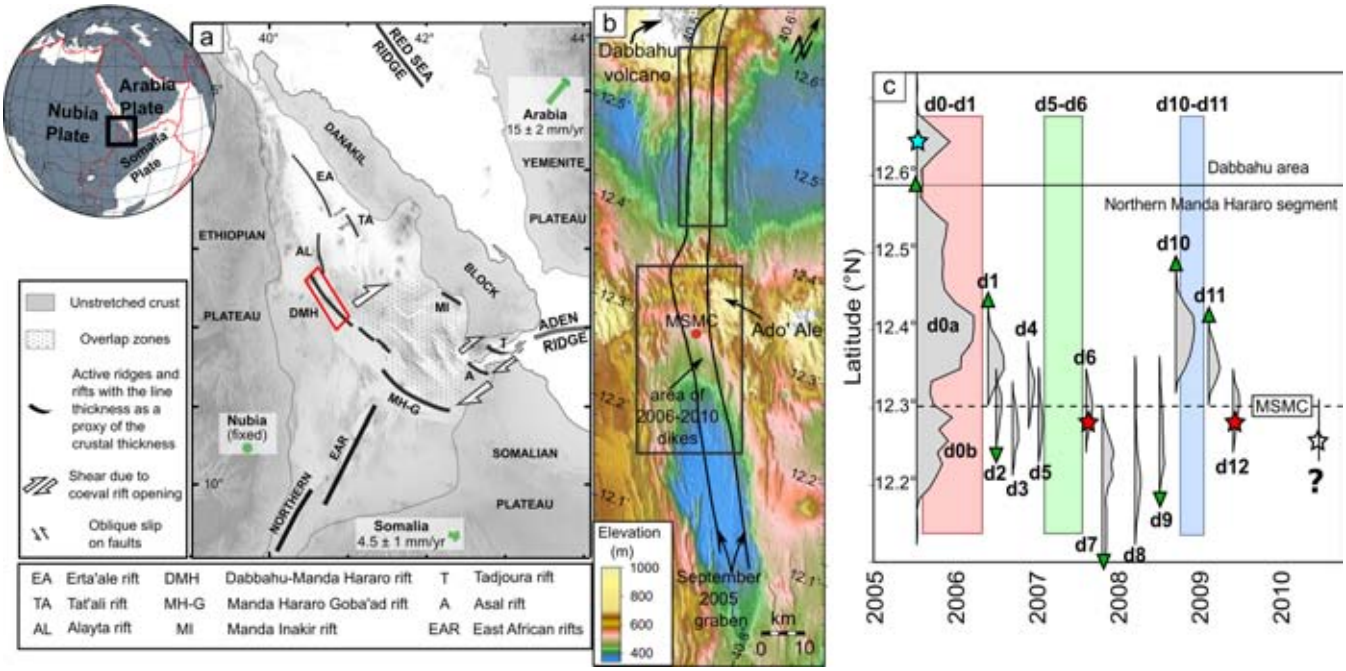

Figure 1. (a) Location and structural scheme of the Afar triple junction, showing a system of magmato-tectonic rifts (tectonic model after Manighetti *et al.* 2001). Green arrows show the Arabia and Somalia plates motions with respect to Nubia (Vigny *et al.* 2006). The Dabbahu–Manda–Hararo rift is indicated by a red rectangle. (b). Topography of the Dabbahu–Manda–Hararo rift with the location of the 2005 September graben (black lines) and the mid-segment magma chamber (MSMC, red dot). The two dark grey rectangles indicate the areas activated during the interdyking periods and analysed in details in this paper. (c) Temporal sequence of dykes injected from 2005 September to 2010 May and represented as a function of latitude (from Grandin *et al.* 2010b). The straight line separates the Dabbahu area from the rift and the dashed line locates the MSMC. The thickness of the grey curves indicates dyke volume per distance unit along the dyke. Stars represent eruptions (cyan: silicic, red: basaltic) and green arrows the direction of seismicity migration during dyke intrusions. This study focuses on the three interdyking periods indicated by the red (d0–d1), green (d5–d6) and blue rectangles (d10–d11).

Downloaded from http://gji.oxfordjournals.org/ by guest on November 26, 2015

The RSR branch in Afar counts four en-echelon magmatic rift segments (Fig. 1a): Erta' Ale, Tat' Ale, Alayta and DMH, localizing most of the extensive deformation associated with the ∼N060°-oriented spreading rate of 15 mm yr^{-1} (Jestin *et al.* 1994; Chu & Gordon 1998; Sella *et al.* 2002; McClusky *et al.* 2003; Vigny *et al.* 2006). The DMH rift segment hosts the Dabbahu stratovolcano (∼10 km diameter) at its northern tip. Like other rift segments in Afar, the DMH encompasses a central volcanic complex. The Ado'Ale (AVC) is of silicic nature and has been intensely dismantled by large systems of normal faults (Fig. 1b; Lahitte *et al.* 2003b). An important change in the orientation of the rift and the fault systems occurs at this part of the rift segment where the normal faults and the main graben are orthogonal to the Arabia/Nubia plate motion along the southern part (Rowland *et al.* 2007), whereas they are oblique to it along the northern area (Rowland *et al.* 2007; Medynski *et al.* 2013).

3 THE 2005–2010 RIFTING EPISODE

The DMH rift was struck by a rifting episode in 2005 September initiated by a seismic sequence involving 15 earthquakes with a magnitude greater than $M_w = 5.0$ (Ayele *et al.* 2007). The surface deformation monitored by InSAR indicates vertical displacements up to 5 m, with a horizontal opening reaching 5–8 m (Wright *et al.* 2006; Grandin *et al.* 2009). Combining InSAR measurements with seismicity analysis revealed a 60-km long dyke intruded at a depth of between 2 and 9 km below the whole segment (Wright *et al.* 2006; Yirgu *et al.* 2006; Ayele *et al.* 2007; Grandin *et al.* 2009) involving a total volume of intruded magma between 1.5 and 2.0 km^3. These results imply a supplementary magma supply from the reservoirs of two volcanoes, Dabbahu and Gabbho, located at the northern tip of the DMH segment and where clear subsidence was observed (Ayele *et al.* 2007, 2009; Grandin *et al.* 2009).

Nine months after this first main event, a new dyke initiated a sequence of 13 smaller dyke intrusions that ended in 2010 May (Hamling *et al.* 2009; Grandin *et al.* 2010b; Fig. 1c). Each one of these dykes was injected after a period of quiescence, called interdyking period, characterized by slow transient ground deformation of smaller amplitude. These lasted between 1 and 11 months (Fig. 1c; Hamling *et al.* 2009, 2010; Grandin *et al.* 2010b). All of these dykes were likely emitted from the mid-segment magma chamber (MSMC) below the AVC (Keir *et al.* 2009; Belachew *et al.* 2011; Grandin *et al.* 2010b, 2011, 2012). They have been described in terms of geometry, opening distribution at depth, volume of intruded magma, stress release and, in certain cases, migration of seismicity (Hamling *et al.* 2009, 2010; Keir *et al.* 2009; Grandin *et al.* 2010b, 2011; Belachew *et al.* 2011, 2013). The volume of magma intruded individually within each of the 13 dykes represents a small fraction of the volume intruded during the event of 2005 September (between 2 per cent and 10 per cent) (Hamling *et al.* 2009, 2010; Grandin *et al.* 2010b) but their cumulative volume is similar to the volume of the first dyke injected in September 2005. These smaller dykes emplaced respectively southward and northward of the MSMC (Hamling *et al.* 2009; Grandin *et al.* 2010b, 2011; Belachew *et al.* 2011, 2013; Fig. 1c) as was observed during the 1975–1984 dyking sequence in the Iceland Krafla segment (Buck *et al.* 2006; Wright *et al.* 2012).

During the interdyking periods, transient deformation was systematically detected by InSAR above the MSMC (Grandin *et al.* 2010a). The monitoring of transient deformation revealed pulses of localized rift opening after the dyke intrusions, followed by an exponentially shaped decay of the opening rate. This signal was interpreted as an indication of the replenishment of the central reservoir involved in feeding the 2005–2009 dykes (Grandin *et al.* 2010a). On the other hand, a sustained deflation of a deep magma reservoir below Dabbahu was observed during the six months following the September 2005 intrusion, with a slow deceleration. Furthermore, a subsidence signal of deep origin was detected within the northern termination of the DMH segment, following a similar temporal evolution. Together, these observations suggest a possible outflow of material from a pre-existing reservoir into, or near, the section of the plate boundary that experienced the massive intrusion of 2005 September (Grandin *et al.* 2010a). This deformation ceased in 2006 June and activity was subsequently restricted to the MSMC area.

The models proposed for explaining the intrusive sequence include faults to explain the subsiding patterns, following the mechanisms proposed for the rifting episodes in Krafla (Iceland) and Asal rifts (Afar) (Ruegg *et al.* 1979; Tarantola *et al.* 1980; Rubin & Pollard 1988; Rubin 1992; Wright *et al.* 2006; Barisin *et al.* 2009; Grandin *et al.* 2009; Hamling *et al.* 2009). Field work carried out after the 2005 September intrusion in the northern part of the rift described a significant amount of opening across numerous normal faults and fissures up to 3 m, with vertical displacements of between 2 m and 5 m (Rowland *et al.* 2007). These observations confirmed estimates of displacement across faults obtained by inversion of geodetic data (Wright *et al.* 2006; Barisin *et al.* 2009; Grandin *et al.* 2009), while also suggesting that the long-term surface deformation was magma-induced (Rowland *et al.* 2007). Most of the models for the 2006–2010 dykes prevent any discussion on the distribution of surface slip along individual faults (whether identified in the topography or not) because of the difficulties involved in unwrapping the interferograms in the main graben, due to the amount of displacement across faults and fissures (Wright *et al.* 2006; Hamling *et al.* 2009, 2010; Grandin *et al.* 2010b). The exceptionally large 2005 September intrusion and the combination of InSAR data and optical images correlation to identify active faults and take them into account in the unwrapping step allowed Grandin *et al.* (2009) to overcome these difficulties partly and describe the behaviour of a large number of the faults activated along the graben during this main intrusion. They observed an opening more pronounced on the north-western margin of the dyke, that they interpret as resulting from the offset of the dyke to the east with respect to the axial depression. The relative locations of the dyke and the pre-existing normal faults could explain why an apparently excessive amount of opening, that is, horizontal displacement, took place along the western dyke border, while the eastern edge behaved more classically with predominant dip-slip motions along faults.

This analysis illustrates a way to evidence magmato-tectonic interactions during a dyking episode. While such observations are very rare, and mostly indirect, they can usually be deduced either from geological outcrops (Mastin & Pollard 1988; Gudmundsson 2003; Gudmundsson & Loetveit 2005; Valentine & Krogh 2006) or from geophysical surveys (Singh *et al.* 2006; Calais *et al.* 2008; Biggs *et al.* 2009; Baer & Hamiel *et al.* 2010; Pallister *et al.* 2010; Nobile *et al.* 2012; Magee *et al.* 2013).

From a long-term perspective, the combination of morphological analysis with dating allowed the identification of the main magmato-tectonic phases for the northernmost part of the rift over the last 100 kyr (Medynski *et al.* 2013). Such a reconstruction suggests that the morphological impact of faulting is strongly controlled by the availability of melt under the Dabbahu volcano (Medynski *et al.* 2013). On a shorter timescale, faults may respond to deep movement of magma and/or to the evolution of the main central

Downloaded from http://gji.oxfordjournals.org/ by guest on November 26, 2015

volcanic reservoir (Sylvester *et al.* 1991; Doubre & Peltzer 2007; Hampel & Hetzel 2008).

4 DATA AND PROCESSING

4.1 InSAR data

Synthetic Aperture Radar Interferometry is a widely used technique to detect surface deformation over large areas. The phase difference between two radar scenes acquired at different times allows the mapping of the surface displacement field with centimetric precision (Massonnet & Feigl 1998; Rosen *et al.* 2000). Such a technique is particularly well adapted to the Afar region, where arid climate limits the coherence loss and allows measurements of the ground movements to an accuracy of a few centimetres per month.

Intrusions of dykes within the upper 10 km of the crust induce surface displacements up to several metres that prevent the retrieval of surface displacements in near field because of an excessive deformation and a large amount of normal faults dissecting the deformation field (Rubin & Pollard 1988; Jónsson *et al.* 1999; Wright *et al.* 2006; Biggs *et al.* 2009; Grandin *et al.* 2009; Lundgren *et al.* 2013). Between dyke injections, the total displacement within the inner part of the rift is smaller. The study of interdyking periods offers a good opportunity to estimate the displacement across faults and its space–time evolution after the intrusion. In addition, an accurate determination of the location of active faults allows the question of their activation to be addressed in relation to magma transfers within the crust (previous dyke emplacement, refilling of the reservoir), which can be detected on the interferograms through broader deformation patterns.

We only took interdyking periods observed by at least two interferograms along both ascending and descending passes into consideration, leading to the analysis of the displacement evolution and the decomposition of the line of sight (LOS) displacement vector into vertical and horizontal components. The SAR data set was divided into two ascending passes (10 scenes for track 28, 4 scenes for track 300) and two descending ones (8 scenes for track 49, 6 scenes for track 464). Images of all tracks were acquired with an incidence angle of $\sim 23^\circ$ (i2), except for the images of track 464 which were acquired with an incidence angle of $\sim 41^\circ$ (i4). The images acquired along the track 464 are therefore more sensitive to the horizontal component of the displacement. The characteristics of each interferogram are detailed in Table 1.

These interferograms were processed at full resolution using the JPL/Caltech ROI_PAC software (Rosen *et al.* 2004). The orbital and topographic contributions were removed using DORIS orbits and the 90 m SRTM Digital Elevation Model (DEM), respectively (Massonnet & Feigl 1998; Hanssen 2001; Zandbergen *et al.* 2003). The phase unwrapping was performed using the branch cut algorithm (Goldstein *et al.* 1988). For areas affected by ground deformation, high fault scarps and displacement along faults could induce significant unwrapping errors. To prevent the phase from being unwrapped across the faults, barriers following the fault tracks were introduced (Doubre & Peltzer 2007; Grandin *et al.* 2010a).

4.2 Estimate of fault displacement

A set of 668 mapped faults was built using the combination of information provided by panchromatic Quickbird images (resolution 60 cm), SPOT-5 images (resolution 2.5 m), DEM generated from SPOT-5 stereo images (resolution 20 m) and InSAR images spanning the post-2005 September period (resolution 20 m) (Grandin *et al.* 2009; Fig. 2). In order to monitor the time and space evolution of displacement across the faults, we extracted the value of the phase difference along profiles normal to the fault direction for all interferograms (see Appendix A for details about the method of the extraction of displacement across faults). Each phase difference estimated across the fault was then converted into LOS displacement. Using interferograms spanning similar time intervals for both ascending and descending tracks, we decomposed the LOS displacement on fault into vertical and horizontal components (see Appendix B for further details). A sign convention is used to discriminate the orientation of displacement on faults: positive for a westward downward movement (reddish) and negative for an eastward downward movement (bluish) (Fig. 3).

Numerous active faults detected in the DMH rift dip westward and exhibit scarps higher than 15 m. The ascending track geometry generates a layover along these west-dipping structures preventing the measurement of the phase difference and thus the determination of the vertical and horizontal components of displacement. The lack of displacement estimate across a few de-correlating faults could lead to underestimating the cumulative displacement calculated for both rift margins hampering therefore their comparison. To avoid this problem, we consider an average angle of the displacement vector as an additional parameter to fix the Z/H ratio, with Z being the vertical displacement and H the horizontal displacement perpendicular to the rift axis. The slip vector for each displacement estimate across the fault is therefore given by alpha $= \arctan(Z/H)$.

The distribution of the displacement angle for all active faults is bimodal with two peaks centred on $10^\circ \pm 10^\circ$ and $60^\circ \pm 20^\circ$, respectively (Appendix C, Fig. C1b). Accordingly, normal faults showing a slip vector of $\sim 10^\circ$ might have been activated more as open fissures than dip-slip faults. The active faults showing a low slip vector are mostly concentrated along the western margin of the dyke (Appendix C, Fig. C1a), whereas the rest of the population of active faults shows dip-slip movements. We therefore use the median values of the slip vector angle to reconstruct the vertical and horizontal displacements for the active faults with a displacement amplitude available only along the LOS direction of the descending track.

Table 1. Characteristics of the interferograms covering the three interdyking periods under study.

	Track (Asc.)	Acquisition date	Bp (m)	Look angle	Track (Desc.)	Acquisition date	Bp (m)	Look angle
December–February 2006 (d0–d1, 1)	t28	060208-051130	180	23°	t49	060210-051202	31	23°
March–April 2006 (d0–d1, 2)	t300	060403-060227	210	23°	t464	060415-060311	325	41°
April–June 2006 (d0–d1, 3)	t300	060612-060403	350	23°	t464	060520-060415	245	41°
January–May 2007 (d5–d6, 1)	t28	070509-070124	25	23°	t464	070505-070120	82	41°
May–July 2007 (d5–d6, 2)	t28	070718-070509	82	23°	t49	070720-070511	105	23°
November–December 2008 (d10–d11, 1)	t28	081224-081119	252	23°	t49	081226-081121	73	23°
December–January 2009 (d10–d11, 2)	t28	090128-081224	28	23°	t49	090130-081226	170	23°

Downloaded from http://gji.oxfordjournals.org/ by guest on November 26, 2015

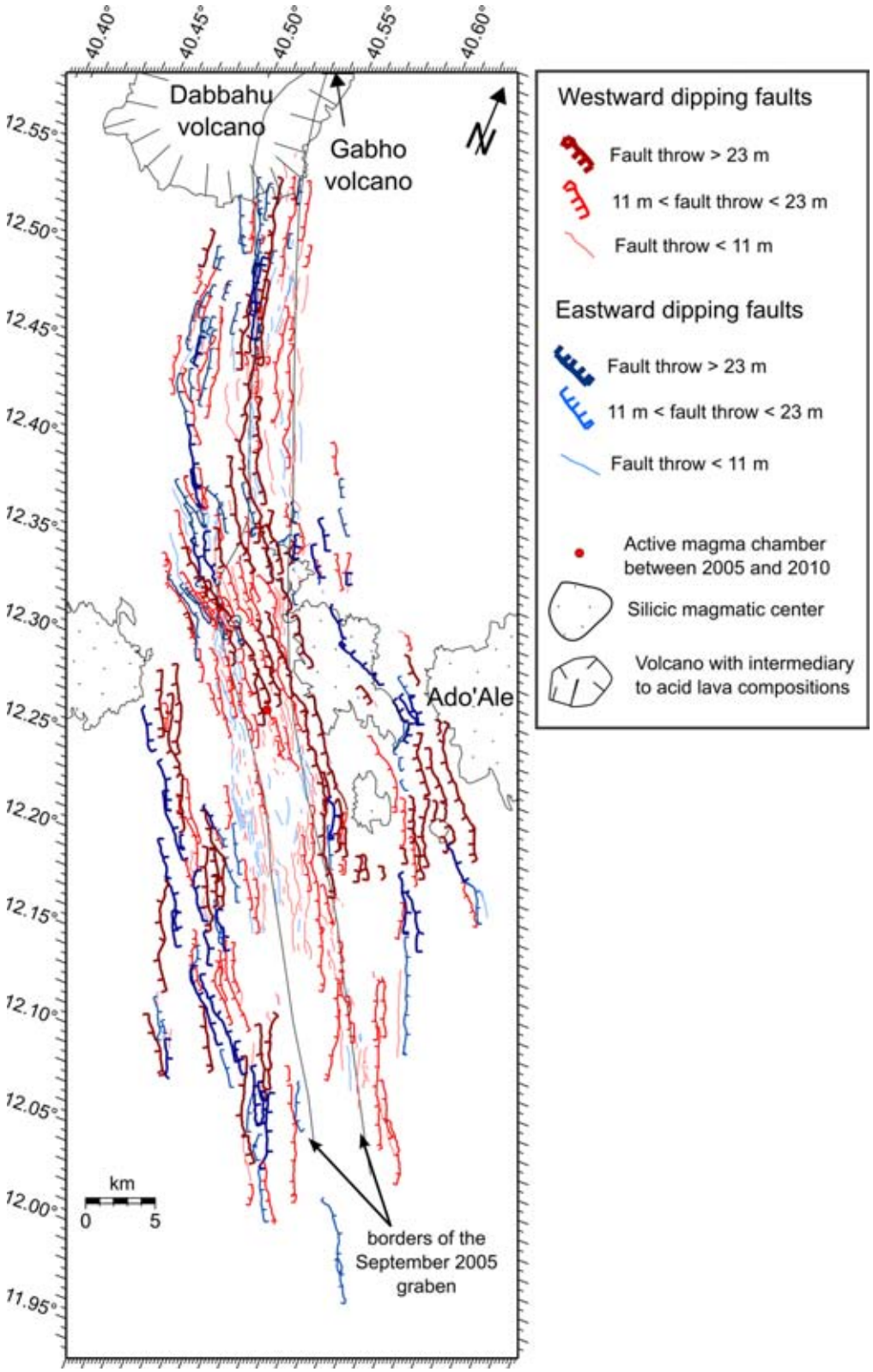

Figure 2. Fault mapping showing 668 faults distributed along the Dabbahu–Manda–Hararo rift, same area as in Fig. 1(b). These faults were mapped using topography, optical and InSAR data (see the text for details). This map includes faults activated during the 2005–2010 rifting episode, and extends moderately on the rift shoulders. The volcanoes and magmatic centres are also represented. The solid black lines indicate the borders of the 2005 September graben.

Downloaded from http://gji.oxfordjournals.org/ by guest on November 26, 2015

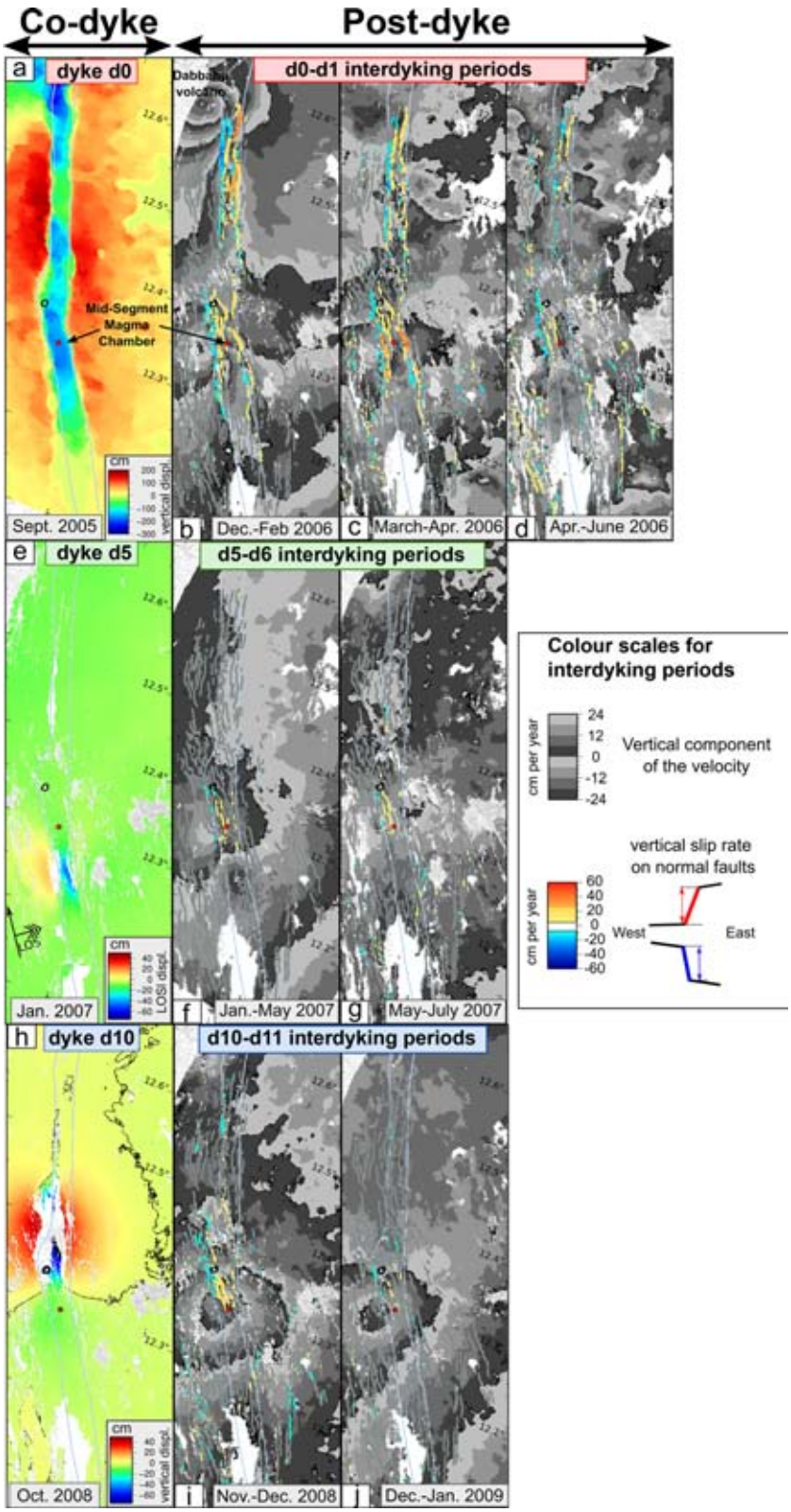

Figure 3. Coloured maps on the left column show codyking displacement fields: vertical displacement field for d0 and d10 intrusions (a and h) and LOS displacement field for d5 (e; the LOS direction being indicated by an arrow since no descending interferogram is available, preventing from retrieving the vertical component). The vertical velocity fields during respective interdyking periods [d0–d1 (b–d), d5–d6 (f and g), d10–d11 (i and j)] are shown on maps with a cyclic grey colour scale. Coloured lineaments superimposed to the velocity field represent activated faults, with a colour scale indicating both the direction and the magnitude of the surface displacement across the fault (yellow-red for west-dipping displacements and blue for east-dipping displacements). The position of the 2005 September graben is indicated by light blue curves and the location of mid-segment magma chamber by a red dot. Concentric fringes at the centre of the rift, associated with the refilling of the main reservoir (Grandin *et al.* 2010b), are observed after each dyke intrusion.

Downloaded from http://gji.oxfordjournals.org/ by guest on November 26, 2015

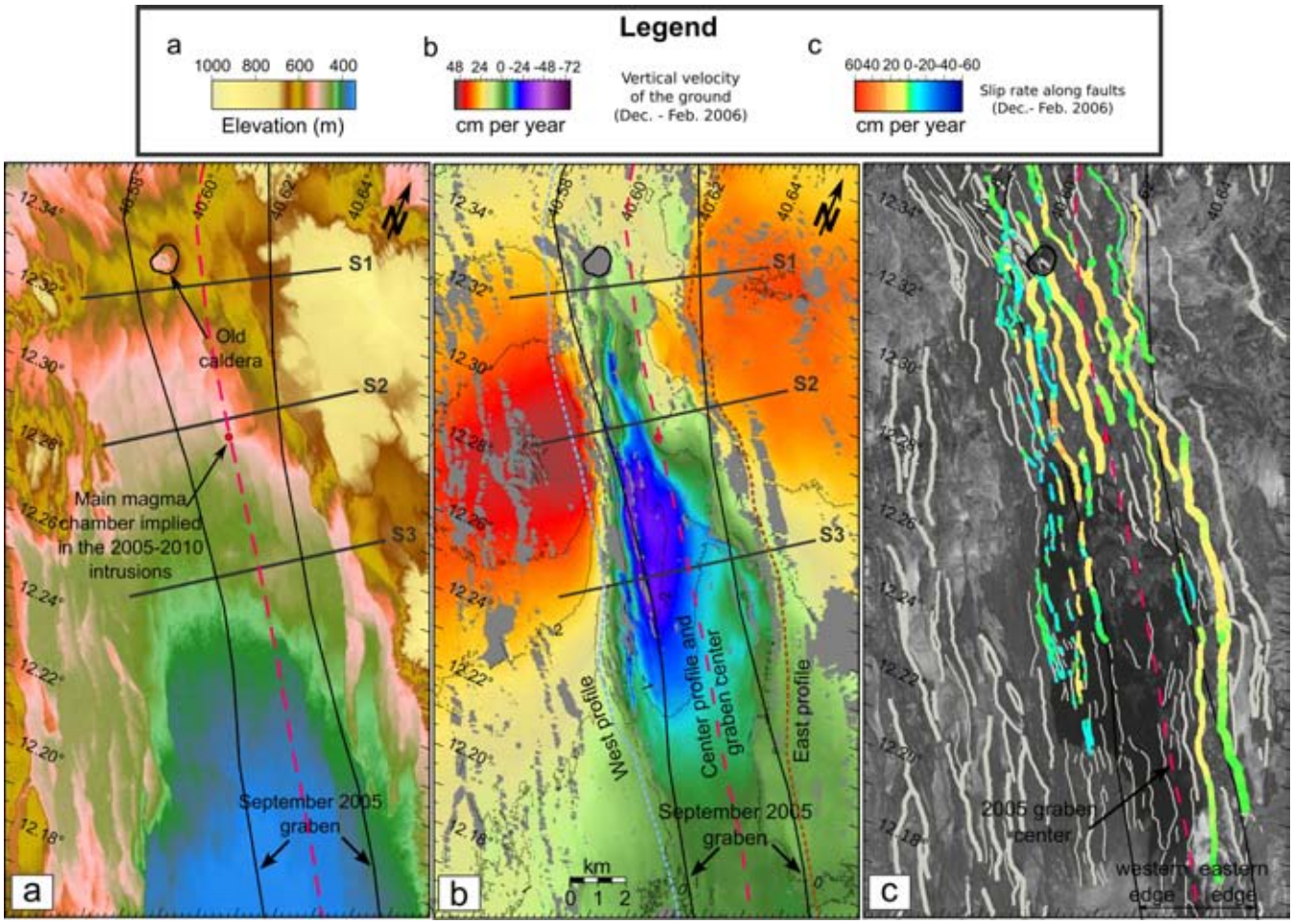

Figure 4. Activated faults in the southern region. Topography (a), vertical velocity field from 2006 December to February (b) and associated displacement rates along the faults printed over a SPOT image (c). The 2005 graben is indicated as reference. The western and eastern edges of the rift are defined with respect to the graben axis (red dashed line), used for the calculations of the cumulative surface displacements across the faults on both margins (Figs 10 and 11). The west, centre and east along-strike profiles (dashed curves) located in (b) are used in Fig. 11. Black lines in (a) and (b) indicate the location of the rift-perpendicular profiles (S1, S2 and S3) shown in Fig. 8. A subsidence is observed south of the present-day reservoir (red dot), while an uplift due to the refilling of this reservoir is observed on the 2005 dyke borders.

5 ACTIVE FAULTS DURING INTERDYKING PERIODS

During the 2005–2010 rifting episode, we consider interdyking periods that follow intrusions showing different deformation patterns: 2005 September (d0), 2007 January (d5) and 2008 October (d10) dykes. The vertical displacement induced by these dykes and the corresponding vertical velocity field during the subsequent interdyking periods are represented in Fig. 3, except for the d5 codyking deformation for which the LOS displacement field is shown instead as only one ascending configuration is available. The displacement across faults is shown for the corresponding interdyking periods. The vertical velocity field during each of the three studied interdyking periods differs significantly from the corresponding codyking displacement field. The remarkable circular fringes uplift pattern at the centre of the rift segment (Fig. 3) has been interpreted as being associated with the refilling of the MSMC after its drainage into the dyke injections (Grandin *et al.* 2010a) with an additional contribution of viscoelastic relaxation (Hamling *et al.* 2014), although the respective importance of these two phenomena remains poorly constrained. This deformation is detailed for the 2006 December–February period in Fig. 4 and similarly for the northern area in Fig. 5. Regardless of the interdyking period considered, the uplift caused by the replenishment of the MSMC matches with an area where faults are systematically slipping after an intrusion (Figs 3 and 4 for details). The magnitude of displacements along faults changes over time (Fig. 6) suggesting that surface slip may be likely triggered by the varying amount of magma replenishing the shallow MSMC (Doubre & Peltzer 2007; Grandin *et al.* 2010a).

At the northern edge of the rift, a pattern of concentric fringes is associated with the subsidence of the deep reservoir of the Dabbahu volcano. This subsidence extends southward into the northern segment of 2005 dyke path and is still detected up to 2006 February (Figs 3 and 5). Grandin *et al.* (2010a) have suggested that these observations, together with the seismological data (Ebinger *et al.* 2008), indicate a continued magma transfer from the Dabbahu deep reservoir into the 2005 dyke path. The subsidence observed in the northern part of 2005 d0 dyke path vanishes with time, concurrent with the decay of the deflation signal at Dabbahu, which is consistent with an outflow mechanism (Fig. 3). Active faults were also observed south–east of the Dabbahu volcano but only during the

Downloaded from http://gji.oxfordjournals.org/ by guest on November 26, 2015

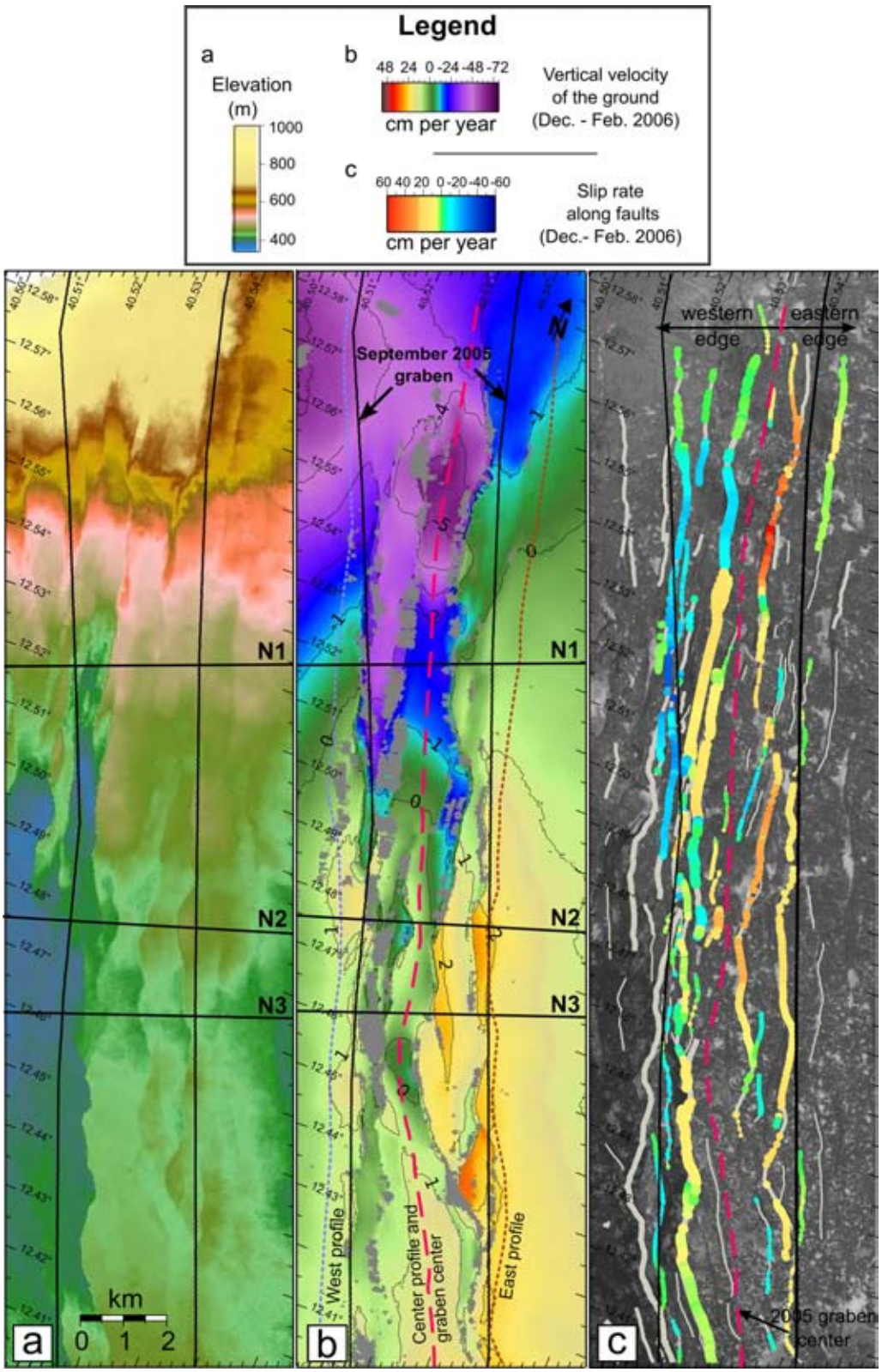

Figure 5. Activated faults for the northern active part of the rift. Topography (a), vertical velocity field from 2006 December to February (b) and associated surface displacement rates across the faults printed over a SPOT image (c). The 2005 September graben is indicated as reference. The western and eastern edges of the rift are defined with respect to the graben axis (red dashed line in b and c), used for the calculations of cumulative surface displacements across the faults on both margins (Figs 9 and 11). The west, centre and east along-strike profiles (dashed curves) located in (b) are used in Fig. 11. Black lines in (a) and (b) locate rift perpendicular profiles (N1, N2 and N3) shown in Fig. 7.

Downloaded from http://gji.oxfordjournals.org/ by guest on November 26, 2015

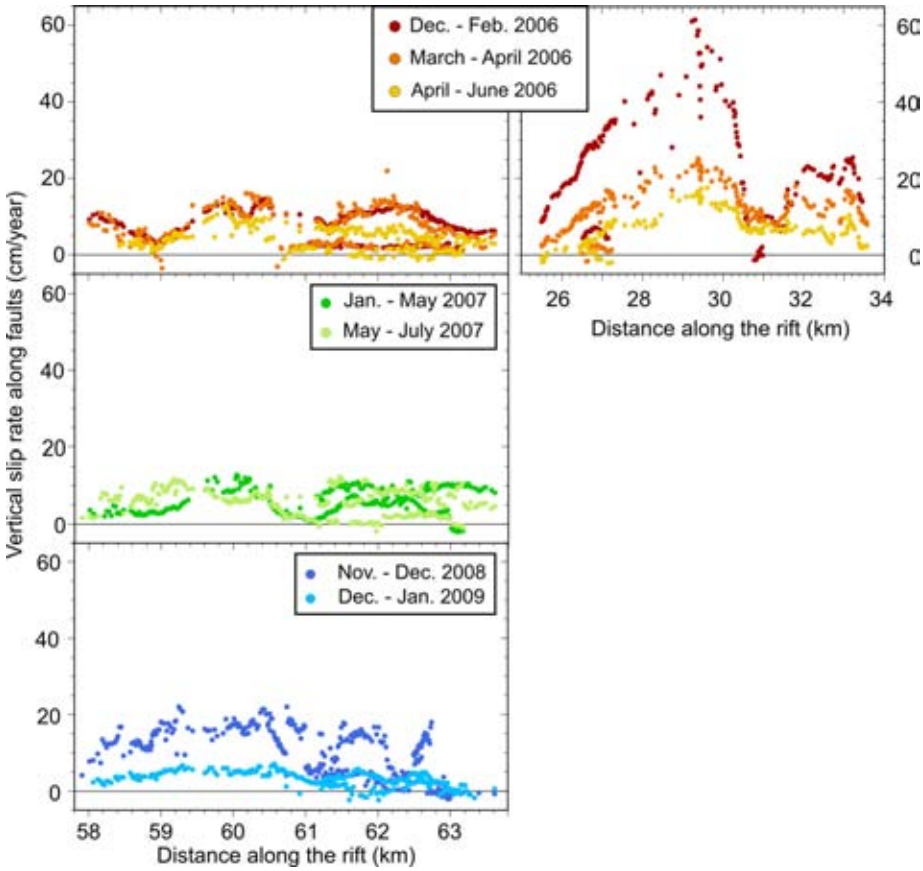

Figure 6. Vertical displacement rates represented for two groups of faults, one located above the mid-segment magma chamber (left column) for which three interdyking periods are shown and one located south-east of Dabbahu volcano (right column) which was only activated after the 2005 September intrusion. Each colour corresponds to a time interval of a studied interdyking period.

six months following the d0 intrusion (Fig. 3). Their displacement rate decreases with time similarly to the velocity field associated with this subsiding area (Figs 3 and 6). Figs 5 and 7 show that this tectonically active area matches exactly with the subsiding band located on the eastern shoulder of the rift, where the d0 dyke was intruded.

6 COMPARISON BETWEEN DISPLACEMENT ALONG FAULTS DURING AND AFTER THE 2005 SEPTEMBER DYKE

6.1 Analysis of ground deformation and displacement distribution

Only the first-order shape of the codyking profiles (Figs 7 and 8) are considered in this analysis as the low-resolution codyking deformation field obtained from the inversion of various data sets (see Grandin *et al.* 2009 for more details) does not allow to discuss the small-scale variations. The profiles extracted across the rift (Figs 7 and 8) show that the faults slipping between 2005 December and 2006 June are located where the 2005 September dyke emplaced. When comparing the width of the bands where faults are slipping during and after the emplacement of the d0 dyke, it appears that the band is ∼30 per cent narrower for the d0–d1 interdyking period, regardless of the active area along the rift considered (Figs 7 and 8). Further examination of the vertical displacements along the profiles (Figs 7 and 8) reveals that the faults slipping during the d0–d1 interdyking period along the western edge of the d0 dyke were activated during the d0 dyke intrusion whereas the faults activated along the eastern edge are not colocated for those same time periods (i.e. during the codyking versus the interdyking). The easternmost fault slipping after the d0 intrusion is shifted by ∼1 km towards the rift centre (Figs 7 and 8). This difference is more pronounced for the northern active area than at the rift centre.

Contrary to what has been suggested by Grandin *et al.* (2009) for the dyke d0, the vertical offsets during the d0–d1 interdyking period are in fact all consistent with the dips of the activated faults. The profiles on Figs 7 and 8 show the distribution of the deformation across the strike of the fault system. They indicate a mechanism of block rotation between faults (particularly clear on profiles N2 and S3). Rotation of blocks allows the overall vertical throw across the western margin of the rift to be consistent with its structural position with respect to the dyke. It accommodates subsidence of the rift axis relative to the western shoulder. However, faults may locally dip in the opposite direction (profile S3, Fig. 8). This mechanism may also have occurred during the codyking period (Grandin *et al.* 2009), but the resolution of the displacement field was too low to capture this feature. The deformation profiles also highlight an asymmetry in the distribution of the opening across the rift (Figs 7 and 8). Most of the opening is accommodated by the westernmost faults and is not equally distributed over the whole system of active faults. This asymmetry is stronger during the interdyking period than during dyking itself (Figs 7 and 8).

Downloaded from http://gji.oxfordjournals.org/ by guest on November 26, 2015

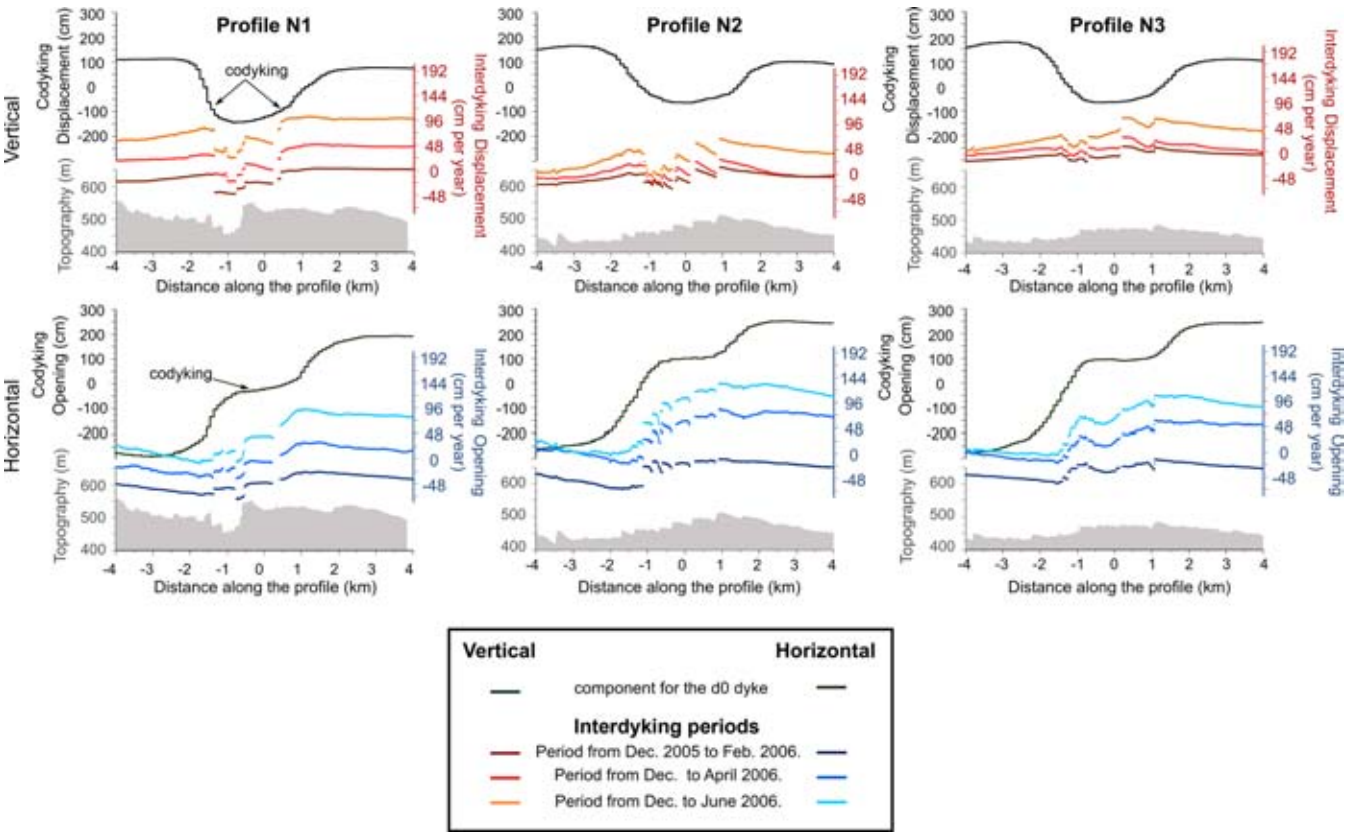

Figure 7. Displacement profiles across the northern part of rift (located in Fig. 5). The black curve shows codyking displacements, while coloured curves show the evolution of the cumulative displacements during d0–d1 interdyking period (from 2005 December to 2006 February, April or June). Top row shows vertical displacements (reddish curves for interdyking) and bottom row shows horizontal component (bluish curves for interdyking). Profile N2 shows a d0–d1 vertical displacement pattern typical of blocks rotations. The staircase patterns in the codyking profiles are due to the lower resolution of the codyking deformation field obtained from inversion of different data sets (see Grandin *et al*. 2009 for more details).

6.2 Analysis of cumulative displacement distribution

Co- and interdyking periods can also be compared by estimating the cumulative distribution of displacement for all active faults located in-between the graben axis and its edges (Figs 9 and 10). The limits of these eastern and western deformation bands are indicated with dashed lines on Figs 4 and 5. For the vertical component, we followed two approaches to estimate the cumulative displacement: (1) the absolute sum of displacement, irrespective of the dip direction and (2) the relative sum that takes the sense of displacement into account and therefore can be used to estimate the actual cumulative vertical offset accommodated by fault displacement through each margin. The differences point out those groups of faults for which the sense of displacement is not consistent with their structural position with respect to the graben axis. These 'anomalous' areas are highlighted in grey on Fig. 11.

Regardless of the area and the component considered, the cumulative displacement is usually higher on the western margin, with a maximum of ∼20 cm, than on the eastern side (∼15 cm). The eastern margin also shows a more segmented pattern (Figs 9 and 10). When the sense of displacement is taken into account, the broad pattern of the vertical cumulative displacement does not change on the eastern side of the rift but changes significantly on its western side (Figs 9 and 10, bottom left column). This difference suggests that most active faults located on the western margin of the d0 graben are west-dipping. This observation is contrary to what is usually expected and may be explained by the fact that d0 dyke emplaced ∼3 km to the east of the rift axial valley, within the rift's eastern shoulder in an area where the topography indicates that the pre-existing faults are dipping towards the west (Figs 1, 4, 5, 7 and 8; Barisin *et al.* 2009; Grandin *et al.* 2009). Finally, even if the distribution of the cumulative displacements along in both vertical and opening components shows initially a shape similar on each margin, the maxima in the opening component shift systematically southward compared to the vertical one. This suggests that the opening may be locally larger than the vertical displacement. This particular behaviour strongly supports a mechanism whereby displacements on faults and opening of fissures are controlled by the movement of a magma body at shallow depth.

Our objective is to evaluate and understand how faults respond to deep forcing and contribute to the deformation field. In Fig. 11, we superimposed the curves corresponding to the surface processes associated with fault activity (relative sum of the vertical cumulative displacement on faults; also shown on Figs 9 and 10, bottom parts) to the curves corresponding to the deep processes, for example, caused by magma transfers at depth (relative deformation across rift shoulders Fig. 11). These two curves corresponding to the deep processes were calculated by taking the difference between profiles extracted in the velocity field along the dyke axis and along its external borders (Figs 4b and 5b for location, Fig. 11 for results). Fig. 11 shows a similarity between the two curves. The peaks of these curves correspond to active areas where transient deformation of magma origin and tectonic deformation occur. They are located above the MSMC and south-east of Dabbahu volcano in the dyke path. These two active regions are separated by a band showing no

Downloaded from http://gji.oxfordjournals.org/ by guest on November 26, 2015

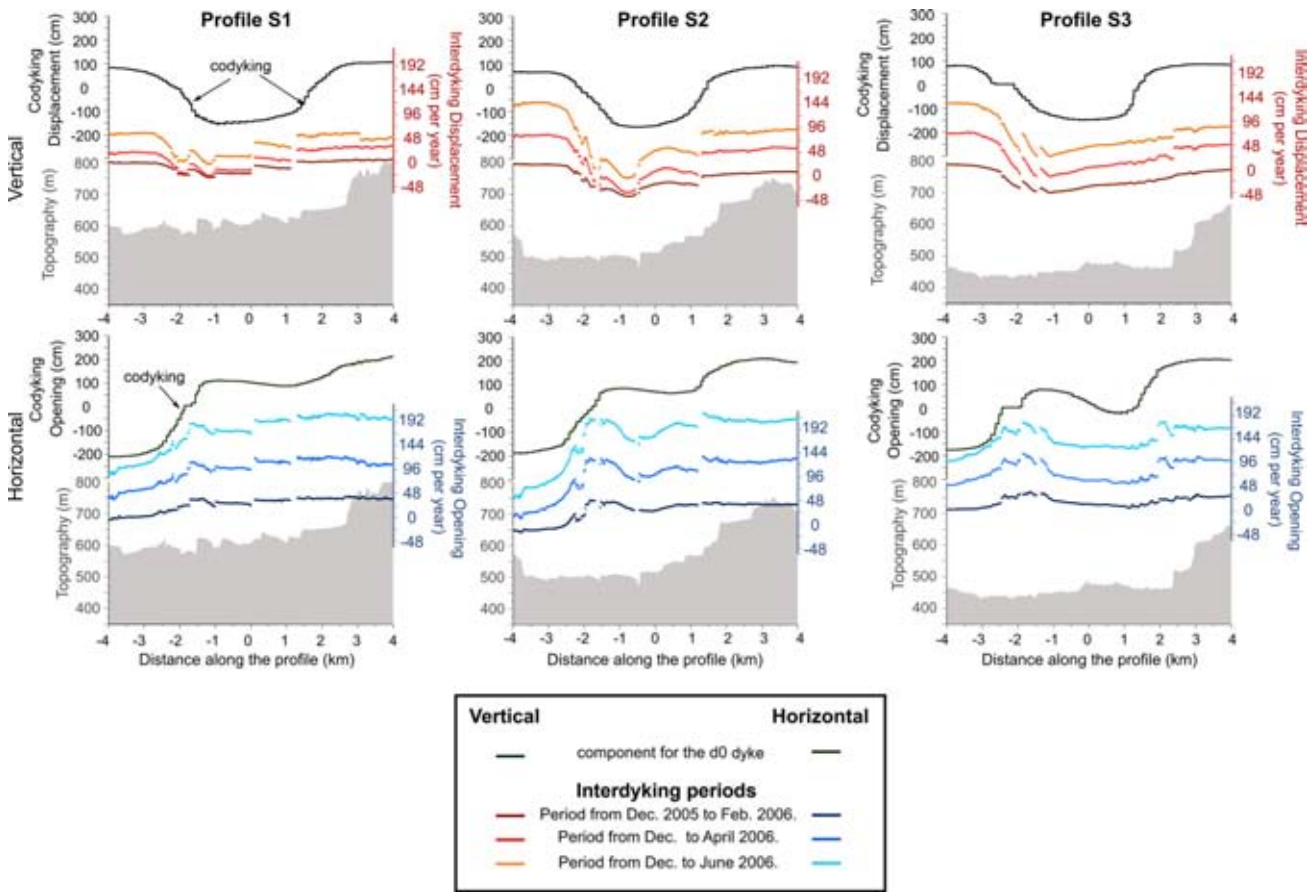

Figure 8. Displacement profiles across the southern part of the rift (located in Fig. 4). The black curve shows codyking displacements, while coloured curves show the evolution of the cumulative displacements during d0–d1 interdyking period (from 2005 December to 2006 February, April or June). Top row shows vertical displacements (reddish curves for interdyking) and bottom row shows horizontal component (bluish curves for interdyking). The staircase patterns in the codyking profiles are due to the lower resolution of the codyking deformation field obtained from inversion of different data sets (see Grandin *et al*. 2009 for more details).

deformation. This suggests that deep processes exert a dominant role in controlling the displacement on faults (both in location and magnitude). However, this similarity is mainly observed for the eastern shoulder of the rift, whatever the active area considered. Differences can be seen on the western edge of the rift, where west-dipping faults accommodate the deformation on the western side of the inflating and propagating magma body, which is in abnormal structural position with respect to the zone of dykes emplacement. There, pre-existing faults and fissures are activated by transfers of magma, but in a sense that is opposite to the total deformation across the shoulder.

7 DISCUSSION

7.1 What triggers surface displacements on faults?

We investigate here the mechanisms inducing the activation of faults during interdyking periods. We considered three time intervals following dyke intrusions at different locations along the rift and involving different volumes of magma, width and depth ranges. Regardless of the interdyking period under consideration (Fig. 3), we observe active faults over areas showing ground deformation. These areas remain the same, whatever the latitudinal location of the dyke intruded previously. We also observe a similar time evolution for both interdyking vertical velocity field and displacement rate along faults (Figs 3 and 6).

Three processes may explain these observations during interdyking periods: (1) a viscoelastic relaxation due to the preceding magma intrusion, (2) a magma transfer within the crust or (3) the dilatation of a magma body already emplaced. Hamling *et al.* (2014) showed recently that a viscoelastic relaxation alone could not explain the interdyking deformation observed at DMH, and confirmed that modeling of deformation requires magma sources along the rift as shown by Grandin *et al.* (2010a). Mantellic viscoelastic relaxation causes large-scale deformation far beyond the rift shoulders and a deformation quite linear over time after many years (Foulger *et al.* 1992; Cattin *et al.* 2005; Hamling *et al.* 2014). In contrary, we highlight here deformation at small scale, mostly located within the axial depression and close to the sources of magma (Dabbahu or MSMC, Figs 3–5). The transient deformation systematically detected at the rift centre after each intrusion can be explained as resulting from the refilling of the MSMC (Grandin *et al.* 2010a). After the d0 intrusion, the lasting seismicity along the northern part of DMH rift, together with a persistent subsidence both at Dabbahu volcano and in the northernmost part of the d0 dyke, were jointly interpreted as being caused by an outflow of magma from the deep reservoir under Dabbahu volcano (Ebinger *et al.* 2008; Grandin *et al.* 2010a). In addition, the high deformation rates affecting the Dabbahu volcano (Figs 3 and 5) and associated with a subsidence pattern reinforce the hypothesis of a magma flow rather than an inflating magma body for which the typical deformation rate is a few millimetres per year (Fialko & Simons 2001). These observations

Downloaded from http://gji.oxfordjournals.org/ by guest on November 26, 2015

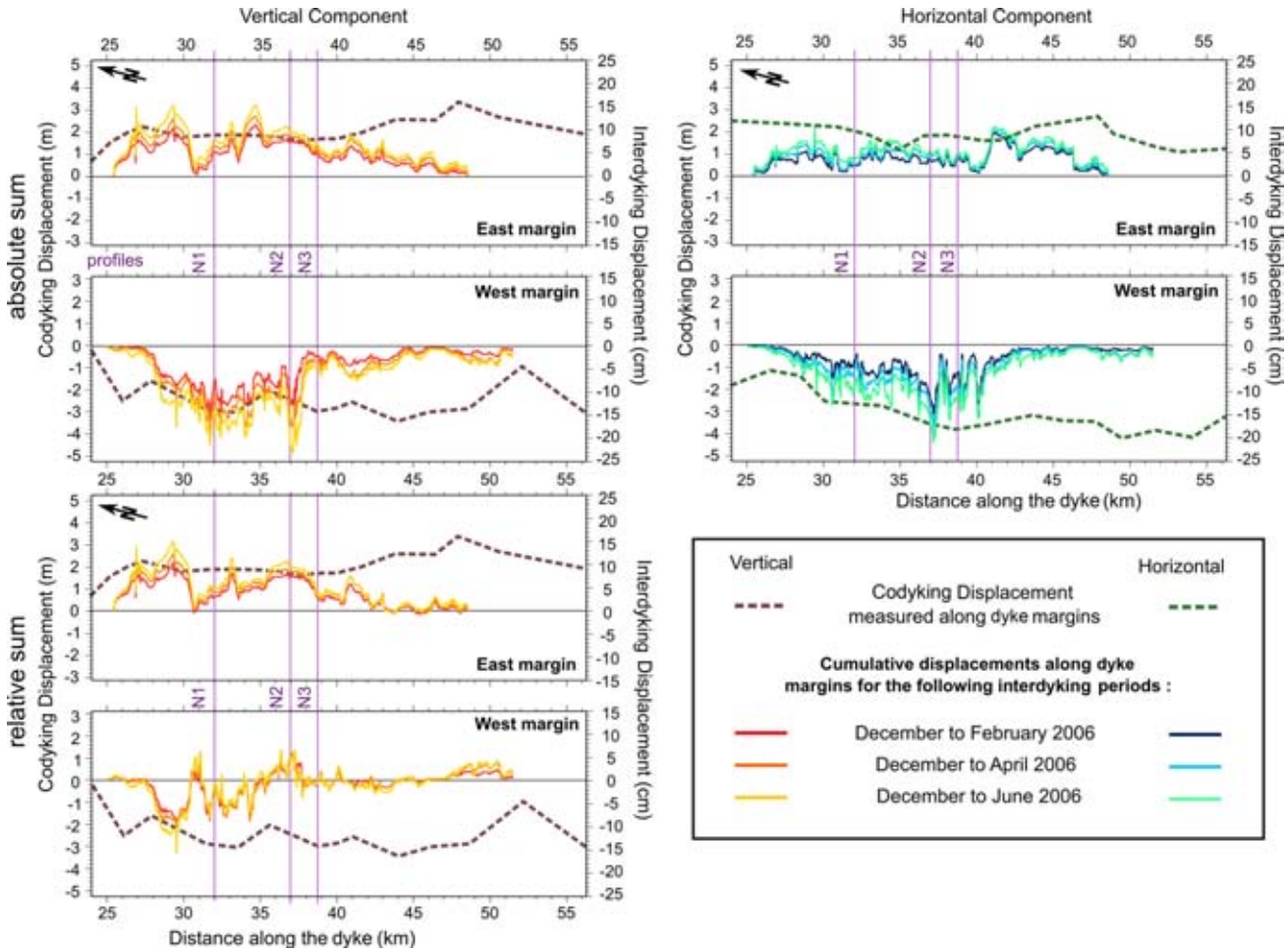

Figure 9. Displacements across both rift margins in the northern activated region. Dashed lines: 2005 September codyking movements. Coloured curves: sum of the displacements on faults belonging to both margins of the rift, during d0–d1 interdyking period (from 2005 December to 2006 February, April or June). Left column depicts vertical offsets and right column horizontal offsets. Two calculations are made for the sum of the vertical movement on faults. Two top left frames: absolute sum that does not take the sense of displacement on faults into account (gives the geodetic moment). Two bottom left frames: relative sum that takes the sense of displacement into account (vertical offset taken on faults through each margin). Profiles of Fig. 5 are indicated by purple vertical lines.

suggest that (1) the ground deformation during the months following each dyke intrusion is generated by magma movements along the rift and (2) that these magma transfers within the crust trigger surface displacements on faults as previously suggested by the modeling of the 1979–1985 period following the Asal rifting episode (Cattin *et al.* 2005). Moreover, the large rates of surface displacement of faults detected, up to 60 cm yr^{-1} after d0 and ~20 cm yr^{-1} on average for the other interdyking periods (Figs 3 and 6), also support this conclusion. These displacement rates are at least two orders of magnitude higher than the long-term displacement rates estimated using dating methods for faults in a similar magmatic context, 0.1–9 mm yr^{-1} (Manighetti *et al.* 1998; Medynski 2013). This comparison suggests that magma accelerates displacement rates at short timescale (Cattin *et al.* 2005; Doubre & Peltzer 2007).

Finally, besides these systematic observations made during the interdyking periods, we studied the specific deformation pattern observed only during the six months following the main intrusion. In the northernmost part of the 2005 September dyke, the subsidence reached values quite similar to those above the Dabbahu volcano, decreasing progressively southward (Fig. 5). This deformation pattern corresponds to the location of the deficit of opening in the 2005 September dyke estimated after inversions of geodetic data (Wright *et al.* 2006; Grandin *et al.* 2009). It has been proposed that this deficit was progressively filled by magma flowing out of the deep Dabbahu reservoir (Grandin *et al.* 2010a). A temporal decay was observed in both displacement rates along the faults and vertical velocity fields (Figs 3 and 6). At the rift centre, the draining of the MSMC into the 2005 September was followed by its progressive replenishment associated with a very limited seismic activity at the rift centre (Ebinger *et al.* 2008; Belachew *et al.* 2011), despite a relative high magma transfer rate (Grandin *et al.* 2010a) which is in agreement with a passive magma influx.

7.2 Comparison of faulting processes during and after a dyke intrusion

We estimated the geometric moment associated with surface displacement across faults for these three interdyking periods in order to compare the energy released by fault activation with that released by dyke intrusion. Most interdyking seismicity at DMH rift occurred at depth shallower than 6 km (Belachew *et al.* 2011) and Rowland *et al.* (2007) proposed that faulting was primarily achieved during dyke events like at DMH rift. Here, we considered fault planes with a 3 km width and a modulus of rigidity of 3×10^{10} Pa. The estimates of geometric moments are presented in Table 2.

Downloaded from http://gji.oxfordjournals.org/ by guest on November 26, 2015

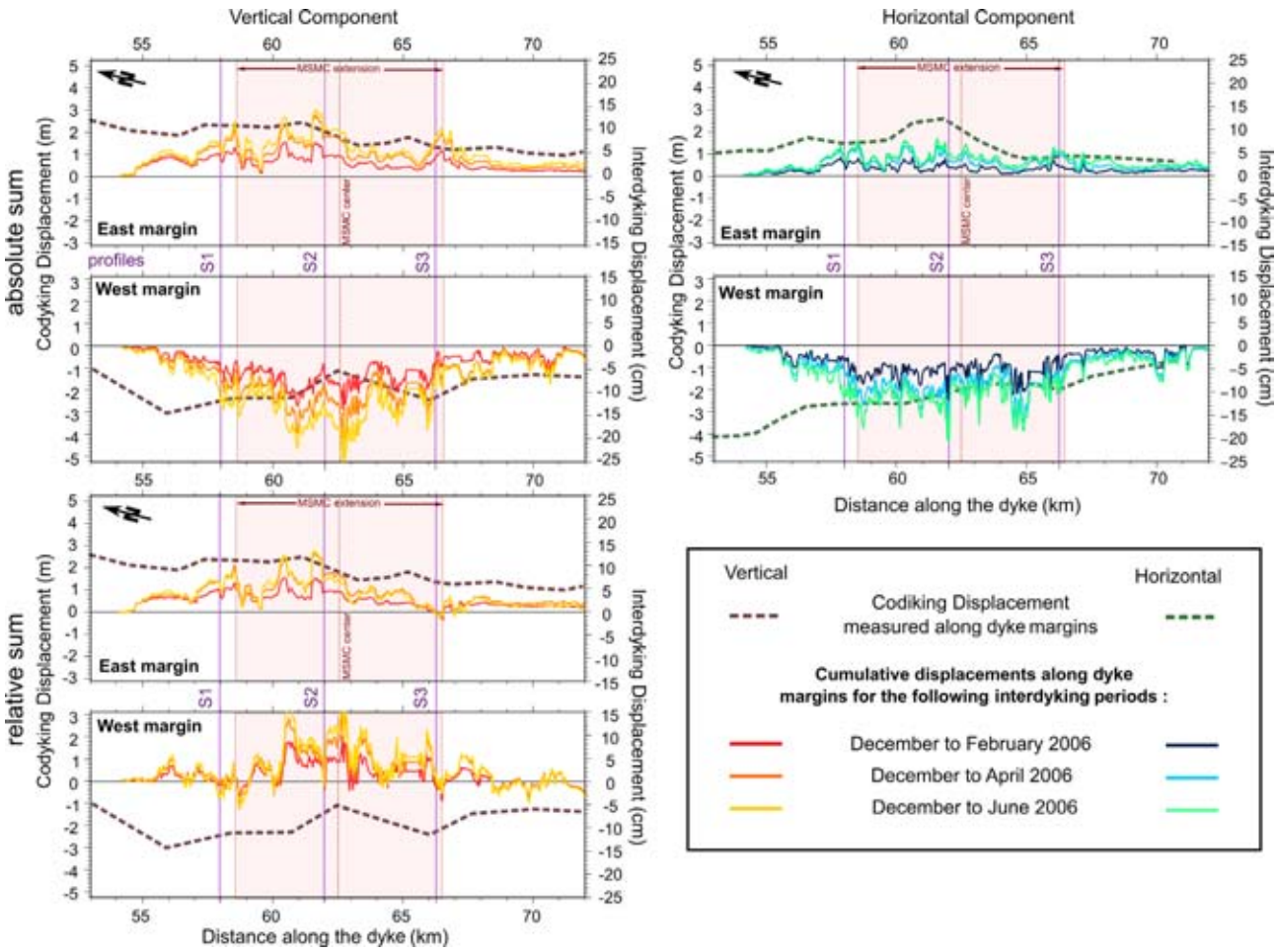

Figure 10. Displacements across both rift margins in the southern activated region. Dashed lines: 2005 September codyking movements. Coloured curves: sum of the displacements on faults belonging to both margins of the rift, during d0–d1 interdyking period (from 2005 December to 2006 February, April or June). Left column depicts vertical offsets and right column horizontal offsets. Two calculations are made for the sum of the vertical movement on faults. Two top left frames: absolute sum that does not take the sense of displacement on faults into account (gives the geodetic moment). Two bottom left frames: relative sum that takes the sense of displacement into account (actual vertical offset taken on faults through each margin). Profiles of Fig. 4 are indicated by purple vertical lines.

They are equivalent to an amount of energy released during a single $M_w = 6.0$ earthquake for the period 2006 December–June, an $M_w = 5.7$ and an $M_w = 5.8$ for the periods 2007 January–July and 2009 November–January, respectively. The energy released during interdyking periods due to faulting (geometric moment) is around one order of magnitude below the energy released during injection and due to dyke opening (geodetic moment, Table 2). This observation is in agreement with the lower amount of induced seismicity during the replenishment phase than during the intrusions (Ebinger *et al.* 2008; Keir *et al.* 2009; Belachew *et al.* 2011; Grandin *et al.* 2011).

This suggests also that displacement along faults is aseismic, similarly as during dyke intrusion as shown by the discrepancy observed between the geodetic and seismic moments (Wright *et al.* 2006; Grandin *et al.* 2009; Belachew *et al.* 2011).

These geometric moments estimated for interdyking periods are as a result, consistent with those for the intrusions (Table 2). More magma is mobilized during a dyke intrusion, more energy is released during dyke emplacement and more energy is then released during the months following the intrusion, allowing the replenishment of the magma chamber. This can be interpreted as the direct consequence of mass conservation since the replenishment of the magma chamber involves a volume of magma quite similar to the one drained out into the dykes.

However, the ratio between the geometric moment and the geodetic moment suggests that energy released by faulting during interperiods accounts for a higher proportion of codyking energy for smaller intrusions (Table 2). The dynamics leading to the replenishment of the magma chamber is probably not similar after each intrusion. Indeed, the flow path, the intrusion depth, the volume of magma mobilized but that left within the reservoir are parameters that change after the various intrusions, especially after small and voluminous dykes. These differences may explain the discrepancies observed between the geodetic and geometric moments.

7.3 What can be inferred from studies of interdyking periods in terms of deep processes and magmato-tectonic interactions ?

The major intrusion of 2005 September and the large deformation detected in the following six months, offer exceptional conditions to compare the nature of the magmatic processes and to study the relationship between faults and magmatism. The analysis of interdyking periods brought details of the distribution of brittle deformation what is difficult to characterize for dyking periods.

Regardless of the area considered, centre or northern part of the rift, we observe a larger component of opening along the western edge of the graben where faults were activated as rotating blocks.

Downloaded from http://gji.oxfordjournals.org/ by guest on November 26, 2015

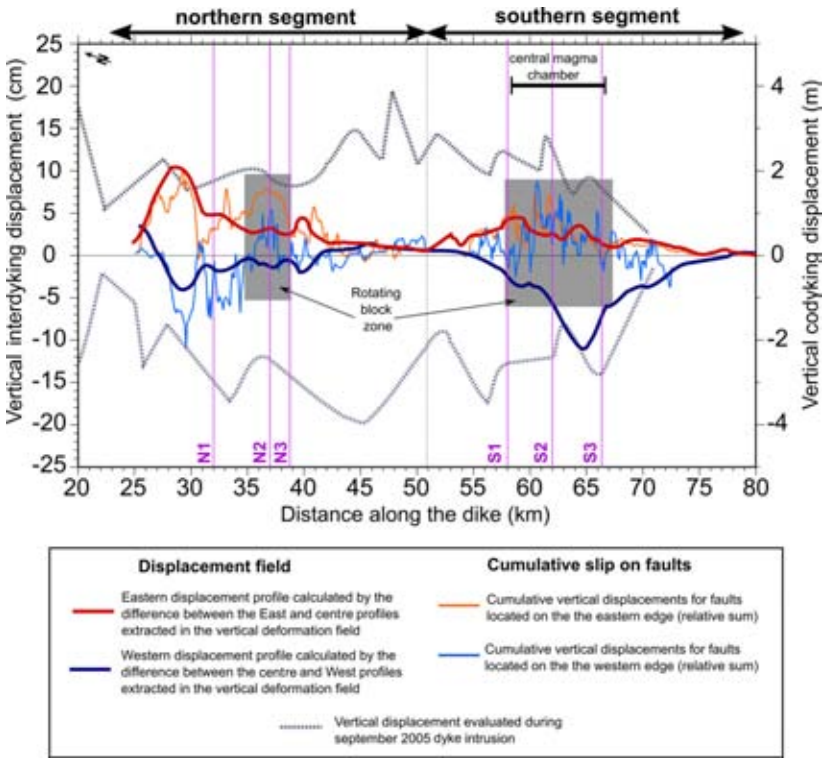

Figure 11. Vertical displacement for both rift margins along the strike of the 2005 September dyke. Dashed lines: codyking vertical displacements across both margins (e.g. relative movement between the graben centre and each shoulder). Red and blue curves: 2005 December–2006 February interdyking displacements across eastern and western margins respectively (e.g. here again difference between the east, west and centre profiles shown in Figs 4 and 5). Orange and cyan thin curves: cumulative vertical displacement on faults belonging to eastern and western margins, respectively (e.g. relative sum shown in Figs 9 and 10). Profiles of Figs 4 and 5 are indicated by purple vertical lines. Pink shaded area depicts the extension of the mid-segment magma chamber (after Grandin *et al.* 2010a). Grey shaded area underlines a zone affected by blocks rotations in the northern active area.

Table 2. Comparisons between energy released during dyke intrusions and that released by faulting during the following interdyking periods. The intrusions of 2005 September (d0), 2007 January (d5) and 2008 October (d10) are compared with the corresponding interdyking periods (d0–d1, d5–d6, d10–d11). M_g geodetic moment, M_0 seismic moment, M geometric moment corresponding to the energy released by faulting. No seismic data were recorded for the 2007 January dyke.

	Dyke d0	d0–d1	Dyke d10	d10–d11	Dyke d5	d5–d6
Dyke volume (km^3)	1.8[b]–2.5[a]		0.17[d]–0.198[c]		0.021[c] –0.045[d]	
M_g (Nm)	8×10^{19} [a]		7.88×10^{18} [d]		2.07×10^{18} [d]	
M_0 (Nm)	6.7×10^{18} [a]		1.781×10^{17} [e]			
M_0/M_g (per cent)	8.3 [a]		2.3 [d,e]			
M (Nm)	3.5×10^{19} [b]	1.1×10^{18}		4.5×10^{17}		3.9×10^{17}
M/M_g (per cent)	1.38	1.38	5.71	5.71	18.84	18.84

[a]Wright *et al.* 2006.
[b]Grandin *et al.* 2009.
[c]Grandin *et al.* 2010b.
[d]Hamling *et al.* 2009, 2010.
[e]Belachew *et al.* 2011.
[f]Grandin *et al.* 2011.

This rotating movement across parallel faults is observed where faults with one single dip orientation were able to release the dyke-induced stresses (Figs 7 and 8). Such a configuration is imposed by the dyke path which was offset to the east with respect to the axial depression even at the rift centre where the offset was only a few kilometres (Figs 4, 5, 7 and 8). These observations are consistent with those made by Grandin *et al.* (2009) for the 2005 September dyke intrusion. Therefore, we suggest that in the absence of conjugated normal faults to release dyke-induced stress, a large component of opening accompanied by a block rotation may be the typical deformation pattern observed at the surface (Fig. 12a) as first proposed by Grandin *et al.* (2009).

Moreover, we also observe a difference between the width of the area affected by brittle deformation for the co- and interdyking periods, with a narrower band of fault activity for the interdyking period (Figs 7 and 8). With regards to the relationship established between the depth range of the dyke and the position of maxima in the deformation field (Pollard *et al.* 1983; Mastin & Pollard 1988; Rubin & Pollard 1988; Rubin 1992), this observation leads us to propose that during the interdyking periods, the magma flow is shallower, likely infiltrating the root of faults and fissures (Fig. 12b). The occupation of fault planes by magma has been directly evidenced from field as well as from geophysical observations (Delaney *et al.* 1986; Gudmundsson & Loetveit 2005; Singh *et al.* 2006;

Downloaded from http://gji.oxfordjournals.org/ by guest on November 26, 2015

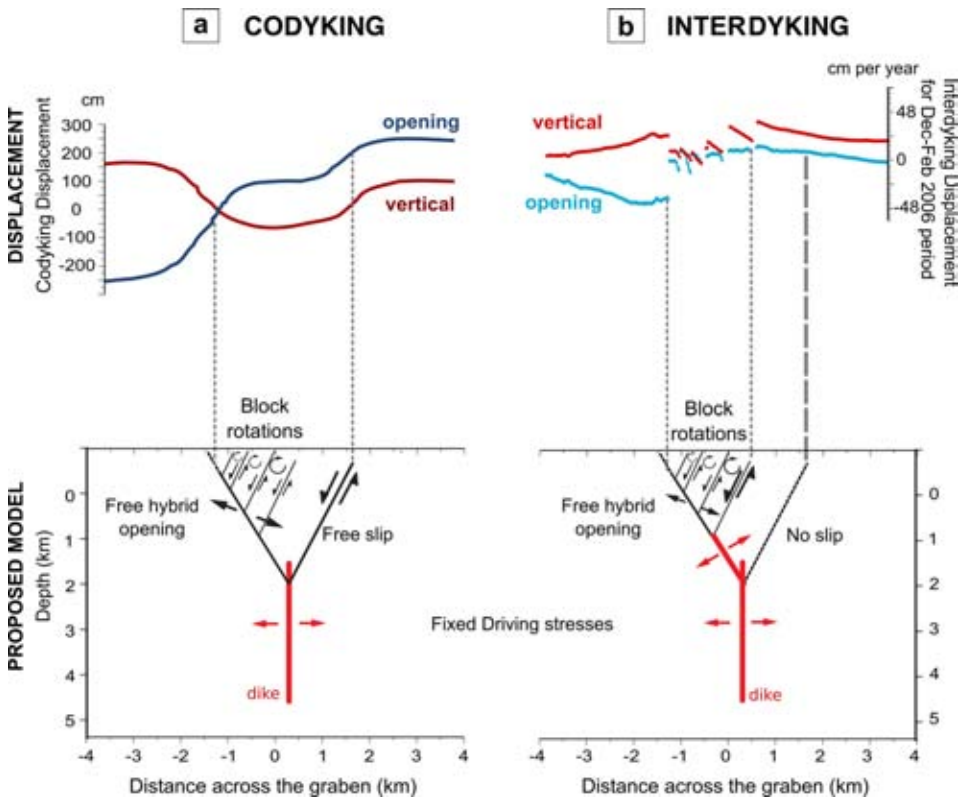

Figure 12. Comparison between the observations and corresponding interpretations for the 2005 codyking deformation (a) and the following six months (b). The common features obtained from the analysis of the displacement distribution and the ground deformation pattern for the interdyking period allow us to complement the model proposed by Grandin *et al.* (2009). The deformation band is narrower and the asymmetry in the opening component is more pronounced during the interdyking period than during the dyke intrusion. We therefore suggest that this deformation pattern is caused by a lens of magma intruded at shallower depths. Adapted after Grandin *et al.* (2009).

Valentine & Krogh 2006; Magee *et al.* 2013). The prevalence of magma transfer at shallow depth might be considered as the cause for the lack of activation of the easternmost fault in the northern segment, which borders the dyke-induced graben of 2005 September (Figs 7 and 12b).

At the rift centre, the spatial distribution of the subsiding area (Figs 4 and 8) shows a southward extend. This deformation pattern may be interpreted as a magma transfer coming from the upper part of the magma chamber and flowing to the d0 dyke path. This may explain why we observe a subsidence pattern superimposed to the uplift until 2006 February, which evidences for the crustal reservoir replenishment (Fig. 4). This hypothesis is also supported by the distribution of active faults located over the subsiding area north of the MSMC and mostly concentrated on the d0 graben edges (Fig. 4). The systematic activation of faults between N12.25° and N12.35° of latitude between the ancient caldera and the central reservoir (Figs 3 and 4) suggests that the magma chamber replenishment affects the same narrow band during the interdyking periods. This observation might reflect the shallow and elongated shape of the reservoir. Nevertheless, all the ground deformation and active faults following dyke intrusions over the 2005–2010 rifting episode should be taken into account, as well as the spatial arrangement of the dykes to better constrain the position and the lateral extension of the central magma chamber.

8 CONCLUSIONS

A rifting episode occurred at DMH rift segment in Ethiopian Afar between 2005 September and 2010 May. It offers a unique opportunity to study the role of faults associated with dyke intrusions and to investigate the relationship between fault activation and magmatism. We focused our analysis on InSAR data for three interdyking periods: 2005 December–2006 June, 2007 January–July and 2008 October–2009 January which followed the intrusion emitted in 2005 September (d0), 2007 January (d5) and 2008 October (d10), respectively. By comparing the locations of the intrusions during the dyking period with both the active faults and the signal of transient deformation over the following months, we show that displacement along faults during interdyking periods is likely triggered by magma transfers within the crust, while viscoelastic relaxation processes play a minor role in the small-scale and near-field surface deformation.

The detailed analysis of the six months following the 2005 September intrusion has shown some common observations in the deformation field as well as in the distribution of brittle deformation, especially an asymmetrical pattern particularly clear during the interdyking period. The interdyking data quality allowed us to complement the model proposed by Grandin *et al.* (2009). We suggest that when the dip of the faults bordering the dyke does not face the dyke centre and therefore does not allow the release of dyke-induced stresses, a significant opening along the outward-facing fault as well as rotating blocks in between the graben borders may be observed. The difference in the width of the deformation band during the co- and interdyking periods is interpreted as a magma transfer at a shallower depth during the interdyking period. Finally, the persistent fault activation between the ancient caldera and the centre of the MSMC may help deciphering the boundaries of the reservoir involved in the different intrusions.

Downloaded from http://gji.oxfordjournals.org/ by guest on November 26, 2015

ACKNOWLEDGEMENTS

We thank the European Space Agency (ESA) for providing Envisat SAR data through the projects AOEZ272, AOEZ720 and PNTS entitled 'Télédétection des déformations transitoires'. SPOT data were acquired through 'Incentive for the Scientific use of Images from the SPOT system' of Centre National des Etudes Spatiales (ISIS 0607–901). The Bonus Qualité Recherche (BQR) of IPGP allowed the acquisition of Quickbird images. The Repeat Orbit Interferometry Package (ROI_PAC) software was provided by Caltech/Jet Propulsion Laboratory (JPL). Most figures were prepared using the Generic Mapping Tool (GMT) software by Wessel & Smith (1991). We would like to thank the two anonymous reviewers and the editor, Prof Trampert, whose insightful comments have greatly improved the manuscript. This paper was supported by the French Agence Nationale pour la Recherche (DoRA project, ANR-09-JCJC-0051–01). This is IPGP contribution number 3687.

REFERENCES

Abdallah, A., Courtillot, V., Kasser, M., Le Dain, A.Y., Lépine, J.C., Robineau, B. & Tarantola, A., 1979. Relevance of Afar seismicity and volcanism to the mechanics of accreting plate boundaries, *Nature,* **282**(5734), 17–23.

Ayele, A., Jacques, E., Kassim, M., Kidane, T., Omar, A., Tait, S. & King, G., 2007. The volcano–seismic crisis in Afar, Ethiopia, starting September 2005, *Earth planet. Sci. Lett.,* **255**(1), 177–187.

Ayele, A., Keir, D., Ebinger, C., Wright, T.J., Stuart, G.W., Buck, W.R. & Sholan, J., 2009. September 2005 mega-dike emplacement in the Manda-Harraro nascent oceanic rift (Afar depression), *Geophys. Res. Lett.,* **36**(20), L20306, doi:10.1029/2009GL039605.

Baer, G. & Hamiel, Y., 2010. Form and growth of an embryonic continental rift: InSAR observations and modelling of the 2009 western Arabia rifting episode, *Geophys. J. Int.,* **182**(1), 155–167.

Barisin, I., Leprince, S., Parsons, B. & Wright, T., 2009. Surface displacements in the September 2005 Afar rifting event from satellite image matching: asymmetric uplift and faulting, *Geophys. Res. Lett.,* **36**(7), L07301, doi:10.1029/2008GL036431.

Belachew, M., Ebinger, C., Coté, D., Keir, D., Rowland, J.V., Hammond, J.O.S. & Ayele, A., 2011. Comparison of dike intrusions in an incipient seafloor-spreading segment in Afar, Ethiopia: seismicity perspectives, *J. geophys. Res.,* **116**(B6), B06405, doi:10.1029/2010JB007908.

Belachew, M., Ebinger, C. & Coté, D., 2013. Source mechanisms of dike-induced earthquakes in the Dabbahu-Manda Hararo rift segment in Afar, Ethiopia: implications for faulting above dikes, *Geophys. J. Int.,* **192**(3), 907–917.

Biggs, J., Amelung, F., Gourmelen, N., Dixon, T.H. & Kim, S.W., 2009. InSAR observations of 2007 Tanzania rifting episode reveal mixed fault and dyke extension in an immature continental rift, *Geophys. J. Int.,* **179**(1), 549–558.

Björnsson, A. & Saemundsson, K., 1977. Current rifting episode in north Iceland, *Nature,* **266,** 318–323.

Björnsson, A., Johnsen, G., Sigurdsson, S., Thorbergsson, G. & Tryggvason, E., 1979. Rifting of the plate boundary in north Iceland, *J. geophys. Res.,* **84,** 3029–3038.

Björnsson, A., 1985. Dynamics of crustal rifting in NE Iceland, *J. geophys. Res.,* **90**(B12), 10 151–10 162.

Blackman, D.K., Nishimura, C.E. & Orcutt, J.A, 2000. Seismoacoustic recordings of a spreading episode on the Mohns Ridge, *J. geophys. Res.,* **105**(B5), 10 961–10 973.

Buck, W.R., 2006. The role of magma in the development of the Afro-Arabian Rift System, *Geol. Soc. Lond. (Spec. Publ.),* **259**(1), 43–54.

Buck, W.R., Einarsson, P. & Brandsdóttir, B., 2006. Tectonic stress and magma chamber size as controls on dike propagation: constraints from the 1975–1984 Krafla rifting episode, *J. geophys. Res*., **111**(B12), B12404, doi:10.1029/2005JB003879.

Calais, E., d'Oreye, N., Albaric, J., Deschamps, A., Delvaux, D., Déverchere, J. & Wauthier, C., 2008. Strain accommodation by slow slip and dyking in a youthful continental rift, East Africa, *Nature,* **456**(7223), 783–787.

Cattin, R., Doubre, C., de Chabalier, J.B., King, G., Vigny, C., Avouac, J.P. & Ruegg, J.C., 2005. Numerical modelling of quaternary deformation and post-rifting displacement in the Asal–Ghoubbet rift (Djibouti, Africa), *Earth planet. Sci. Lett.,* **239**(3), 352–367.

Chu, D. & Gordon, R.G., 1998. Current plate motions across the Red Sea, *Geophys. J. Int.,* **135**(2), 313–328.

De Chabalier, J.B. & Avouac, J.P., 1994. Kinematics of the Asal Rift (Djibouti) determined from the deformation of Fieale Volcano, *Science,* **265**(5179), 1677–1677.

Delaney, P.T., Pollard, D.D., Ziony, J.I. & McKee, E.H., 1986. Field relations between dikes and joints: emplacement processes and paleostress analysis, *J. geophys. Res.,* **91**(B5), 4920–4938.

Doubre, C. & Peltzer, G., 2007. Fluid-controlled faulting process in the Asal Rift, Djibouti, from 8 yr of radar interferometry observations, *Geology,* **35**(1), 69–72.

Dziak, R.P., Smith, D.K., Bohnenstiehl, D.R., Fox, C.G., Desbruyeres, D., Mat-sumoto, H., Tolstoy, M. & Fornari, D.J., 2004. Evidence of a recent magma dike intrusion at the slow spreading Lucky Strike segment, Mid-Atlantic Ridge, *J. geophys. Res.,* **109**(B12), B12102, doi:10.1029/2004JB003141.

Ebinger, C.J. & Casey, M., 2001. Continental breakup in magmatic provinces: an Ethiopian example, *Geology,* **29**(6), 527–530.

Ebinger, C.J., Keir, D., Ayele, A., Calais, E., Wright, T.J., Belachew, M. & Buck, W.R., 2008. Capturing magma intrusion and faulting processes during continental rupture: seismicity of the Dabbahu (Afar) rift, *Geophys. J. Int.,* **174**(3), 1138–1152.

Efron, B. & Tibshirani, R., 1986. Bootstrap methods for standard errors, confidence intervals, and other measures of statistical accuracy, *Stat. Sci.,* **1**(1), 54–75.

Einarsson, P. & Brandsdottir, B., 1980. Seismological evidence for lateral magma intrusion during the July 1978 delfation of the Krafla Volcano in NE-Iceland, *J. Geophys.,* **47,** 160–165.

Einarsson, P., 1991. The Krafla rifting episode 1975–1989, in *Náttúra Mývatns (The Nature of Lake Mývatn),* pp. 97–139, eds Gardarsson, A. & Einarsson, A., Icelandic Nature Science Society, Reykjavik.

Fialko, Y. & Simons, M., 2001. Evidence for on-going inflation of the Socorro magma body, New Mexico, from Interferometric synthetic aperture radar imaging, *Geophys. Res. Lett.,* **28**(18), 3549–3552.

Foulger, G.R., Jahn, C.H., Seeber, G., Einarsson, P., Julian, B.R. & Heki, K., 1992. Post-rifting stress relaxation at the divergent plate boundary in Northeast Iceland, *Nature,* **358**(6386), 488–490.

Goldstein, R.M., Zebker, H.A. & Werner, C.L., 1988. Satellite radar interferometry: two-dimensional phase unwrapping, *Radio Science,* **23**(4), 713–720.

Grandin, R., Socquet, A., Binet, R., Klinger, Y., Jacques, E., de Chabalier, J.B. & Pinzuti, P., 2009. September 2005 Manda Hararo-Dabbahu rifting event, Afar (Ethiopia): constraints provided by geodetic data, *J. geophys. Res.,* **114**(B8), B08404, doi:10.1029/2008JB005843.

Grandin, R., Socquet, A., Doin, M.P., Jacques, E., de Chabalier, J.B. & King, G.C.P., 2010a. Transient rift opening in response to multiple dike injections in the Manda Hararo rift (Afar, Ethiopia) imaged by time-dependent elastic inversion of interferometric synthetic aperture radar data, *J. geophys. Res.,* **115**(B9), B09403, doi:10.1029/2009JB006883.

Grandin, R., Socquet, A., Jacques, E., Mazzoni, N., de Chabalier, J.B. & King, G.C.P., 2010b. Sequence of rifting in Afar, Manda-Hararo rift, Ethiopia, 2005–2009: time-space evolution and interactions between dikes from interferometric synthetic aperture radar and static stress change modeling, *J. geophys. Res.,* **115**(B10), B10413, doi:10.1029/2009JB000815.

Grandin, R., Jacques, E., Nercessian, A., Ayele, A., Doubre, C., Socquet, A. & King, G.C.P., 2011. Seismicity during lateral dike propagation: insights from new data in the recent Manda Hararo–Dabbahu rifting episode (Afar, Ethiopia), *Geochem. Geophys. Geosyst.,* **12**(4), Q0AB08, doi:10.1029/2010GC003434.

Downloaded from http://gji.oxfordjournals.org/ by guest on November 26, 2015

Grandin, R., Socquet, A., Doubre, C., Jacques, E. & CP King, G., 2012. Elastic thickness control of lateral dyke intrusion at mid-ocean ridges, *Earth planet. Sci. Lett.,* **319,** 83–95.

Gudmundsson, A., 2003. Surface stresses associated with arrested dykes in rift zones, *Bull. Volc.,* **65**(8), 606–619.

Gudmundsson, A. & Loetveit, I., 2005. Dyke emplacement in a layered and faulted rift zone, *J. Volc. Geotherm. Res.,* **144**(1–4), 311–327.

Hamling, I.J., Ayele, A., Bennati, L., Calais, E., Ebinger, C.J., Keir, D. & Yirgu, G., 2009. Geodetic observations of the ongoing Dabbahu rifting episode: new dyke intrusions in 2006 and 2007, *Geophys. J. Int.,* **178**(2), 989–1003.

Hamling, I.J., Wright, T.J., Calais, E., Bennati, L. & Lewi, E., 2010. Stress transfer between thirteen successive dyke intrusions in Ethiopia, *Nat. Geosci.,* **3**(10), 713–717.

Hamling, I.J., Wright, T.J., Calais, E., Lewi, E. & Fukahata, Y., 2014. InSAR observations of post-rifting deformation around the Dabbahu rift segment, Afar, Ethiopia, *Geophys. J. Int.,* **197**(1), 33–49.

Hammond, J.O.S., Kendall, J.M., Stuart, G.W., Keir, D., Ebinger, C., Ayele, A. & Belachew, M., 2011. The nature of the crust beneath the Afar triple junction: evidence from receiver functions, *Geochem. Geophys. Geosyst.,* **12**(12), doi:10.1029/2011GC003738.

Hampel, A. & Hetzel, R., 2008. Slip reversals on active normal faults related to the inflation and deflation of magma chambers: numerical modeling with application to the Yellowstone-Teton region, *Geophys. Res. Lett.,* **35**(7), L07301, doi:10.1029/2008GL033226.

Hanssen, R.F., 2001. *Radar Interferometry: Data Interpretation and Error Analysis,* Vol. 2, Springer.

Hayward, N.J. & Ebinger, C.J., 1996. Variations in the along-axis segmentation of the Afar Rift system, *Tectonics,* **15**(2), 244–257.

Jestin, F., Huchon, P. & Gaulier, J.M. 1994. The Somalia plate and the East African Rift System: present-day kinematics, *Geophys. J. Int.,* **116**(3), 637–654.

Jónsson, S., Zebker, H., Cervelli, P., Segall, P., Garbeil, H., Mouginis-Mark, P. & Rowland, S., 1999. A shallow-dipping dike fed the 1995 flank eruption at Fernandina Volcano, Galápagos, observed by satellite radar interferometry, *Geophys. Res. Lett.,* **26**(8), 1077–1080.

Keir, D., Hamling, I.J., Ayele, A., Calais, E., Ebinger, C., Wright, T.J. & Bennati, L., 2009. Evidence for focused magmatic accretion at segment centers from lateral dike injections captured beneath the Red Sea rift in Afar, *Geology,* **37**(1), 59–62.

Lahitte, P., Gillot, P.Y., Kidane, T., Courtillot, V. & Bekele, A., 2003a. New age constraints on the timing of volcanism in central Afar, in the presence of propagating rifts, *J. geophys. Res.,* **108**(B2), 2123, doi:10.1029/2001JB001689.

Lahitte, P., Gillot, P.Y. & Courtillot, V., 2003b. Silicic central volcanoes as precursors to rift propagation: the Afar case, *Earth planet. Sci. Lett.,* **207**(1), 103–116.

Le Dain, A., Robineau,, B. & Tapponnier, P., 1979. Les effets tectoniques de l'événement sismique et volcanique de novembre 1978 dans le rift d'Asal-Ghoubbet, *Bull. Soc. Geol. Fr.,* **22,** 817–822.

Lépine, J.C., Ruegg, J.C. & Anis, A.M., 1980. Sismicité du rift d'Asal-Ghoubbet pendant la crise sismo-volcanique de novembre 1978, *Bull. Soc. Geol. Fr.,* **6,** 809–816.

Lundgren, P., Poland, M., Miklius, A., Orr, T., Yun, S.H., Fielding, E. & Owen, S., 2013. Evolution of dike opening during the March 2011 Kamoamoa fissure eruption, Kīlauea Volcano, Hawaii, *J. geophys. Res.,* **118**(3), 897–914.

Magee, C., Jackson, C.A.L. & Schofield, N., 2013. The influence of normal fault geometry on igneous sill emplacement and morphology, *Geology,* **41**(4), 407–410.

McClusky, S., Reilinger, R., Mahmoud, S., Sari, D.B. & Tealeb, A., 2003. GPS constraints on Africa (Nubia) and Arabia plate motions, *Geophys. J. Int.*, **155**(1), 126–138.

Makris, J. & Ginzburg, A., 1987. The Afar depression: transition between continental rifting and sea-floor spreading, *Tectonophysics,* **141**(1), 199–214.

Manighetti, I., Tapponnier, P., Gillot, P.Y., Jacques, E., Courtillot, V., Armijo, R. & King, G., 1998. Propagation of rifting along the Arabia-Somalia plate boundary: Into Afar, *J. geophys. Res.,* **103**(B3), 4947–4974.

Manighetti, I., Tapponnier, P., Courtillot, V., Gallet, Y., Jacques, E. & Gillot, P.Y., 2001. Strain transfer between disconnected, propagating rifts in Afar, *J. geophys. Res.,* **106**(B7), 13 613–13 665.

Massonnet, D. & Feigl, K.L., 1998. Radar interferometry and its application to changes in the Earth's surface, *Rev. Geophys.,* **36**(4), 441–500.

Mastin, L.G. & Pollard, D.D., 1988. Surface deformation and shallow dike intrusion processes at inyo craters, Long Valley, California, *J. geophys. Res.,* **93**(B11), 13 221–13 235.

Medynski, S., 2013. Interactions entre phénomènes tectoniques et magmatiques encontexte d'extension: l'exemple du segment de rift de Dabbahu, *PhD thesis*, Université de Lorraine, Nancy.

Medynski, S., Pik, R., Burnard, P., Williams, A., Vye-Brown, C., Ferguson, D. & Calvert, A., 2013. Controls on magmatic cycles and development of rift topography of the Manda Hararo segment (Afar, Ethiopia): insights from cosmogenic ^{3}He investigation of landscape evolution, *Earth planet. Sci. Lett.,* **367,** 133–145.

Nobile, A., Pagli, C., Keir, D., Wright, T.J., Ayele, A., Ruch, J. & Acocella, V., 2012. Dike-fault interaction during the 2004 Dallol intrusion at the northern edge of the Erta Ale Ridge (Afar, Ethiopia), *Geophys. Res. Lett.,* **39**(19), L19305, doi:10.1029/2012GL053152.

Nooner, S.L., Bennati, L., Calais, E., Buck, W.R., Hamling, I.J., Wright, T.J. & Lewi, E. 2009. Post-rifting relaxation in the Afar region, Ethiopia, *Geophys. Res. Lett.,* **36**(21), L21308, doi:10.1029/2009GL040502.

Pagli, C., Wang, H., Wright, T.J., Calais, E. & Lewi, E. 2014. Current plate boundary deformation of the Afar rift from a 3-D velocity field inversion of InSAR and GPS, *J. geophys. Res.,* **119**(11), 8562–8575.

Pallister, J.S., McCausland, W.A., Jónsson, S., Lu, Z., Zahran, H.M., El Hadidy, S. & Moufti, M.R., 2010. Broad accommodation of rift-related extension recorded by dyke intrusion in Saudi Arabia, *Nat. Geosci.,* **3**(10), 705–712.

Pollard, D.D., Delaney, P.T., Duffield, W.A., Endo, E.T. & Okamura, A.T., 1983. Surface deformation in volcanic rift zones, *Tectonophysics,* **94**(1), 541–584.

Rosen, P.A., Hensley, S., Joughin, I.R., Li, F.K., Madsen, S.N., Rodriguez, E. & Goldstein, R.M., 2000. Synthetic aperture radar interferometry, *Proc. IEEE,* **88**(3), 333–382.

Rosen, P.A., Hensley, S., Peltzer, G. & Simons, M., 2004. Updated repeat orbit interferometry package released, *EOS, Trans. Am. geophys. Un.,* **85**(5), 47.

Rowland, J.V., Baker, E., Ebinger, C.J., Keir, D., Kidane, T., Biggs, J. & Wright, T.J., 2007. Fault growth at a nascent slow-spreading ridge: 2005 Dabbahu rifting episode, Afar, *Geophys. J. Int.,* **171**(3), 1226–1246.

Rubin, A.M., 1992. Dike-induced faulting and graben subsidence in volcanic rift zones, *J. geophys. Res.,* **97**(B2), 1839–1858.

Rubin, A.M. & Pollard, D.D., 1988. Dike-induced faulting in rift zones of Iceland and Afar, *Geology,* **16**(5), 413–417.

Ruegg, J.C., Lepine, J.C., Tarantola, A. & Kasser, M., 1979. Geodetic measurements of rifting associated with a seismo-volcanic crisis in Afar, *Geophys. Res. Lett.,* **6**(11), 817–820.

Sella, G.F., Dixon, T.H. & Mao, A., 2002. REVEL: A model for recent plate velocities from space geodesy, *J. geophys. Res.,* **107**(B4), 2081, doi:10.1029/2000JB000033.

Singh, S.C., Crawford, W.C., Carton, H., Seher, T., Combier, V., Cannat, M. & Miranda, J.M., 2006. Discovery of a magma chamber and faults beneath a Mid-Atlantic Ridge hydrothermal field, *Nature,* **442**(7106), 1029–1032.

Sylvester, A.G., Byrd, J.O.D. & Smith, R.B., 1991. Geodetic evidence for aseismic reverse creep across the Teton fault, Teton Range, Wyoming, *Geophys. Res. Lett*., **18**(6), 1083–1086.

Tarantola, A., Ruegg, J.C. & Lépine, J.C., 1979. Geodetic evidence for rifting in Afar a brittle-elastic model of the behaviour of the lithosphere, *Earth planet. Sci. Lett.,* **45**(2), 435–444.

Tarantola, A., Ruegg, J.C. & Lepine, J.P., 1980. Geodetic evidence for rifting in Afar, 2. Vertical displacements, *Earth planet. Sci. Lett.,* **48**(2), 363–370.

Tiberi, C., Ebinger, C., Ballu, V., Stuart, G. & Oluma, B., 2005. Inverse models of gravity data from the Red Sea-Aden-East African rifts triple junction zone, *Geophys. J. Int.,* **163**(2), 775–787.

Tryggvason, E., 1984. Widening of the Krafla fissure swarm during the 1975–1981 volcano-tectonic episode, *Bull. Volc.,* **47**(1), 47–69.

Downloaded from http://gji.oxfordjournals.org/ by guest on November 26, 2015

Valentine, G.A. & Krogh, K.E., 2006. Emplacement of shallow dikes and sills beneath a small basaltic volcanic center–the role of pre-existing structure (Paiute ridge, southern Nevada, USA Earth planet, *Sci. Lett.,* **246**(3), 217–230.

Vigny, C., Huchon, P., Ruegg, J.C., Khanbari, K. & Asfaw, L.M., 2006. Confirmation of Arabia plate slow motion by new GPS data in Yemen, *J. geophys. Res.*, **111**(B2), B02402, doi:10.1029/2004JB003229.

Wessel, P. & Smith, W.H.F., 1991. *The GMT-System Version 2.0 Technical Reference and Cookbook,* Scripps Institution of Oceanography, University of California, San Diego.

Wright, T.J., Parsons, B.E. & Lu, Z., 2004. Toward mapping surface deformation in three dimensions using InSAR, *Geophys. Res. Lett.,* **31**(1), L01607, doi:10.1029/2003GL018827.

Wright, T.J., Ebinger, C., Biggs, J., Ayele, A., Yirgu, G., Keir, D. & Stork, A., 2006. Magma-maintained rift segmentation at continental rupture in the 2005 Afar dyking episode, *Nature,* **442**(7100), 291–294.

Wright, T.J. *et al.*, 2012. Geophysical constraints on the dynamics of spreading centres from rifting episodes on land, *Nat. Geosci.,* **5**(4), 242–250.

Yirgu, G., Ababa, A. & Ayele, A., 2006. Recent seismovolcanic crisis in northern Afar, Ethiopia, *EOS, Trans. Am. geophys. Un.,* **87**(33), 325–329.

Zandbergen, R., Otten, M., Righetti, P.L., Kuijper, D. & Dow, J.M., 2003. Routine operational and high-precision orbit determination of Envisat, *Adv. Space Res.,* **31**(8), 1953–1958.

APPENDIX A: EXTRACTION OF FAULT DISPLACEMENT AMPLITUDE

Displacement on normal faults induces a downward movement that produces a discontinuity along the fault in the interferometric phase field (Fig. A1a). To quantify the magnitude of the displacement along the 668 mapped faults, we first estimated the direction of the profiles used for the extraction of the displacement (Figs A1a and b). This direction is defined by the extreme points of each individual fault which determine the global fault strike, since most faults are primarily linear. Then, the profiles are extracted every 15.5 m on average along the fault, as the number of profiles depending on the fault length, with an orientation perpendicular to the fault direction (Fig. A1b). Because the location of the fault results from a mapping based on a combination of various images having different resolutions, we need to relocate precisely the phase discontinuity along profiles. We use a bootstrap approach (Efron & Tibshirani 1986) based on the first derivative. As the interferometric phase is affected by topographic errors and layover/shadowing across the fault scarps, especially for those with the highest cumulative throw, a region of 3 pixels across the fault scarps was systematically masked in order to avoid such errors in the estimates of relative displacements (Fig. A1c). Once the position of the fault is determined precisely (red point, Fig. A1c), the magnitude of the displacement is quantified subtracting the closest points to the fault belonging to the two linear regressions fitting the displacement on each side of the fault (Fig. A1c).

APPENDIX B: DETERMINATION OF THE VERTICAL COMPONENT OF-THE DISPLACEMENT

InSAR measurements give the ground displacement component only along the radar LOS. The full displacement vector can therefore not be resolved with a unique InSAR measurement. To resolve this, we use a combination of InSAR measurements from different imaging geometries (ascending and descending passes). The following equations describe the relation between the LOS measurement d_{LOS} and the displacement vector d, $d = [dN, dE, dV]$:

$$d_{\mathrm{LOS}} = \cos\theta_{\mathrm{inc}} dV - \sin\theta_{\mathrm{inc}}\ d_{\mathrm{HORIZ}} \tag{1}$$

with dN, dE, dV being the components in north, east and vertical direction, respectively. θ_{inc} is the incidence angle and d_{HORIZ} is the projection of the horizontal displacements on the azimuth look direction:

$$d_{\mathrm{HORIZ}} = \cos\alpha\, dN \pm \sin\alpha\, dE \tag{2}$$

with α, the heading azimuth of the satellite orbit.

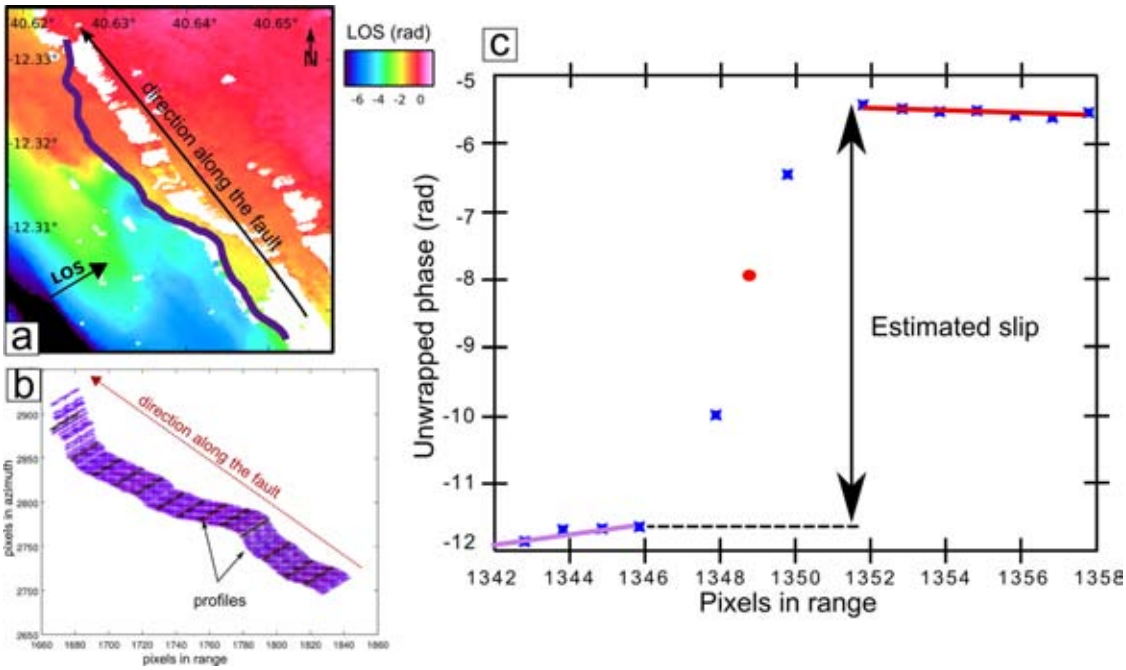

Figure A1. (a) Zoom on an active fault located along DMH rift: a gradient across the fault evidences the dip-slip movement in an interferogram. (b) Profiles are extracted perpendicularly to the main direction of the faults. They are presented here in radar geometry. (c) On this profile, the fault centre is located (red point) using the bootstrap method. The two linear regressions are used to estimate the fault slip.

Downloaded from http://gji.oxfordjournals.org/ by guest on November 26, 2015

In this study, deciphering the nature of the movements across the faults (how much faults have slipped vertically or/and opened) is crucial to investigate the interactions between faults and magma. We aimed therefore at considering time intervals for which both ascending and descending images were available, allowing us to decompose the LOS measurement into vertical component and the horizontal one perpendicular to the rift. The rift azimuth is almost oriented north-south, which implies that expected movements along normal faults will essentially be vertical and/or oriented east-west. Moreover, the near-polar orbit of the ENVISAT satellite makes the north component particularly difficult to determine (Wright *et al.* 2004). We therefore considered the horizontal movement in the north-south direction as negligible. This assumption ($dN \sim 0$) enabled us to resolve the system of equations using observations from only two different look directions.

APPENDIX C: DETAILS OF THE SLIP VECTOR

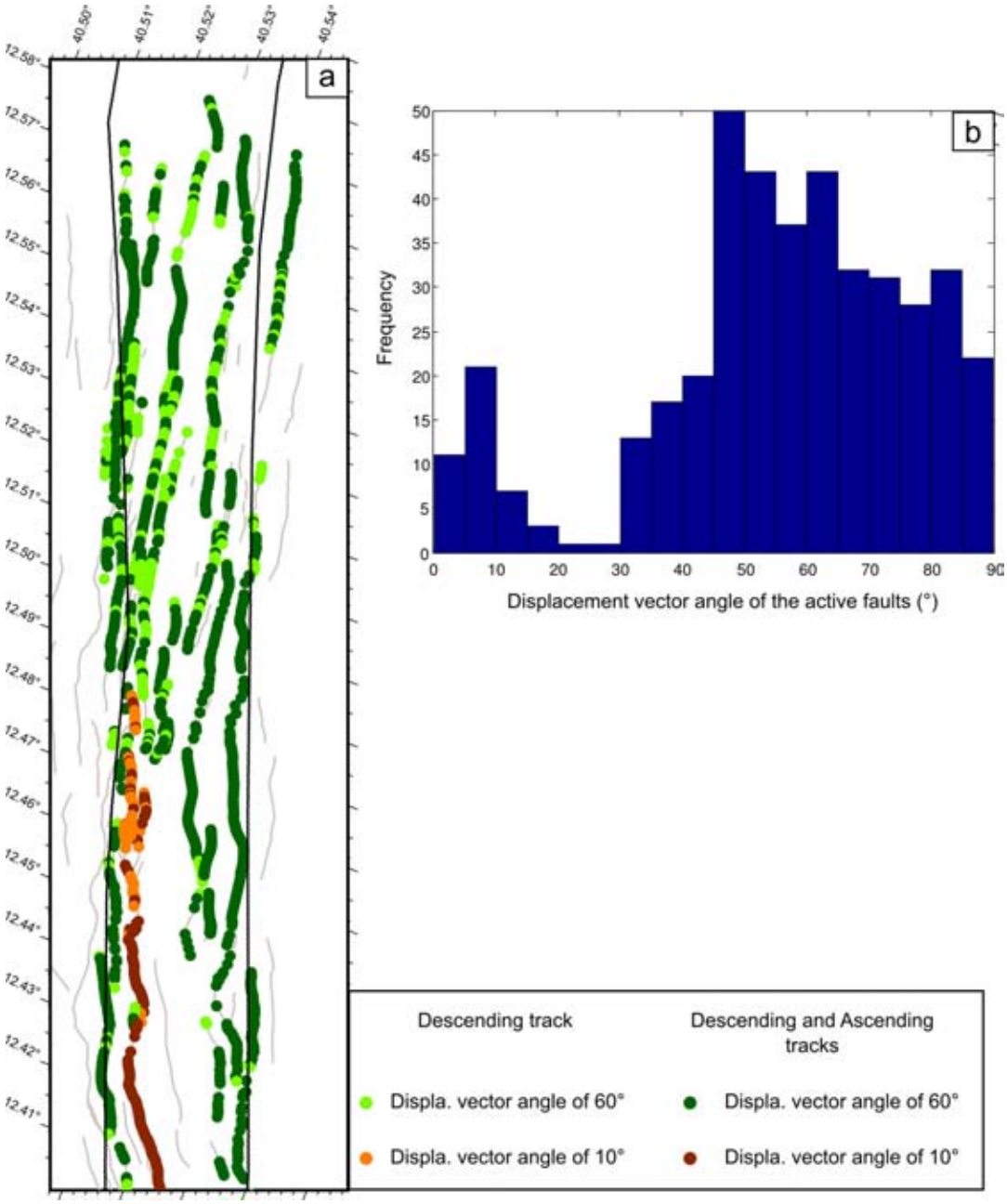

Figure C1. (a) Zoom on the northern part of the rift where each colour point corresponds to a measuring point of the displacement along the faults. The darker contrasts of the colour points indicate that the displacement is available for both ascending and descending tracks, while the lighter ones are only available in a single configuration, preventing the decomposition of the displacement estimate into vertical and horizontal components. The colour of the measuring point shows the angle of the displacement vector. (b) The histogram shows a bimodal distribution of the displacement vector angle for the active faults. Both median angles of 10° and 60° were used to calculate the vertical and horizontal components for areas where only one the descending estimate of the displacement was available.

Downloaded from http://gji.oxfordjournals.org/ by guest on November 26, 2015